Spin-Flop-Induced Coarsening of Antiferromagnetic Domains in a Fe/Cr Multilayer

D.L. Nagy, L. Bottyán, L. Deák, E. Szilágyi, M. Major
(KFKI Research Institute for Particle and Nuclear Physics, Budapest, Hungary)
J. Dekoster, M. Major (K.U. Leuven, Instituut voor Kernen Stralingsfysica, Leuven, Belgium)
H.J. Lauter, V. Lauter-Pasyuk (Institut Laue-Langevin, Grenoble, France)
V. Lauter-Pasyuk (Technische Universität München, Garching, Germany)
O. Nikonov, A. Petrenko (Frank Laboratory of Neutron Physics, JINR, Dubna, Russia)

Antiferromagnetically (AF) coupled metallic multilayers [1] have received much attention in recent years due to their relevance in fundamental science and technology alike. The archetype Fe/Cr system shows oscillatory interlayer coupling [2, 3] and giant magnetoresistance (GMR) [4]. The transport behavior of coupled multilayers is markedly affected by static and dynamic properties of the domain structure. Nevertheless, our knowledge on the AF domain structure of coupled multilayers is still much limited.

Off-specular polarized neutron reflectometry (PNR) [5, 6] and off-specular synchrotron Mössbauer reflectometry (SMR) [7] have proved to be useful tools to estimate the AF domain size distribution. A microdomain structure was invoked to describe the broad off-specular sheets found by PNR at the AF reflection of Fe/Cr multilayers in applied magnetic field [6]. In the present report, which is the summary of a part of a more detailed publication [8], we will show that a domain coarsening takes place in low magnetic fields when the system passes the spin-flop transition. This is a direct evidence that magnetocrystalline anisotropy plays a key role in the dependence of the domain structure on the magnetic field history.

The sample used in this study was an MBE-grown $MgO(001)/[^{57}Fe(26Å)/Cr(13Å)]_{20}$ superlattice. An irreversible spin-flop transition takes place in this AF-coupled multilayer of fourfold in-plane anisotropy, as observed with PNR [9] and SMR [10], when a magnetic field of $H_{SF} = (14\pm2)$ mT is applied parallel to the easy axis along which the layer magnetizations are lying. At this critical field the magnetic energy overcomes the energy A of the fourfold in-plane magnetocrystalline anisotropy and the layer magnetizations jump to the perpendicular easy axis. This alignment is retained as long as the external field does not change its direction.

The PNR experiment was performed at the SPN-1 polarized neutron reflectometer of the Dubna pulsed reactor IBR-2. The sample was placed between the poles of an electromagnet applying an in-plane field parallel to the linear polarization of the incoming neutrons. Two spin flippers one before and one after the sample could flip the polarization of both the

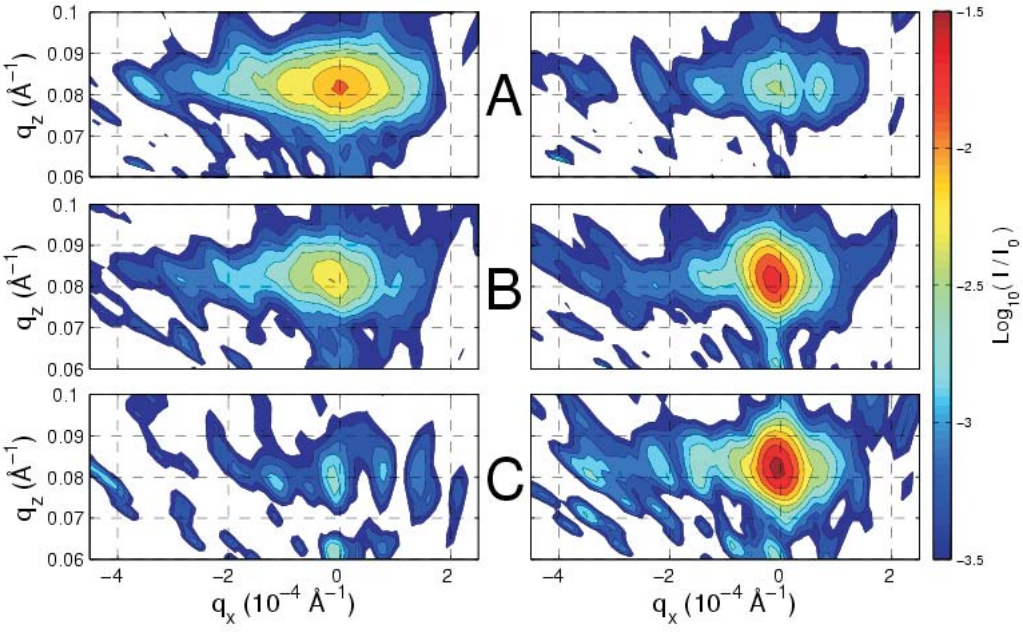

Fig.1. Intensity maps I/I_0 of specular and off-specular scattered neutrons from a MgO(001)/[^{57}Fe(26Å)/Cr(13Å)]$_{20}$ multilayer in a magnetic field of A) 7 mT, B) 14.2 mT and C) 35 mT in the non-spin-flip (R^-, left side) and in the spin-flip (R^+, right side) channels as a function of the scattering vector components q_x and q_z.

incoming and of the scattered neutrons. A Soller-type supermirror stack analyzed the polarization of the scattered neutrons. A position-sensitive detector detected the neutrons reflected by the analyzer so that the scattered neutrons were mapped in the $q_z q_x$ plane of the scattering vector **q** in all (++, +-, -+ and --) channels. The measurements were performed in a static magnetic field at (286±2) K.

The sample was previously saturated in a field of 2.1 T and placed into the reflectometer with magnetization parallel/antiparallel to the incoming neutron polarization. Below the spin-flop transition the AF reflection only appeared in the ++ and -- channels and consisted of a broad diffuse sheet. During the transition the AF reflection shows up in all channels. While in the ++ and --channels the AF reflection consists only of a diffuse sheet, in the +-and -+ channels its main part is specular scattering (cf. Fig. 1). Having passed the transition, the AF reflection is only observed in the +-and -+ channels and is mainly specular. The diffuse sheets correspond to the 'ripened' [11] microdomains formed after decreasing the magnetic field from saturation. The average domain size, i.e., the autocorrelation length of the layer magnetization in this state is ξ = 800 nm. The presence of a narrow specular reflection after passing the spin-flop transition shows the appearance of large domains with $\xi > 5$ μm. During the spin-flop transition, a mixed state of mutually perpendicular small and large domains exists. The domain coarsening has also been observed with off-specular SMR [8].

In conclusion, we observed the magnetic-field-history dependent antiferromagnetic domain structure of an MgO(001)/[^{57}Fe(26Å)/Cr(13Å)]$_{20}$ superlattice by off-specular PNR. It was found that releasing the field from full saturation in easy direction results in a small-domain state. However, large size

patch domains are formed from these primary small domains on passing the spin-flop transition. This gives a new insight into the nature of the domain-coarsening transition by showing that its condition is not the equilibrium of the Zeeman energy with the domain wall energy, but *the equilibrium of the Zeeman energy with the anisotropy energy*. It is only this equilibrium that permits the much smaller domain wall energy to shape the domain structure. Out of this equilibrium the Zeeman energy or the anisotropy energy whichever is greater will stabilize the already existing domain structure.

The authors acknowledge helpful discussions with Drs. B. Croonenborghs, B. Degroote, E. Kunnen, O. Leupold, J. Meersschaut, R. Rüffer, H. Spiering, and K. Temst.

References:

1. P. Grünberg, R. Schreiber, Y. Pang, M.B. Brodsky, H. Sowers, *Phys. Rev. Lett.* **57,** 2242 (1986).
2. S.S.P. Parkin, N. More, K.P. Roche, *Phys. Rev. Lett.* **64,** 2304 (1990).
3. J. Unguris, R.J. Celotta, D.T. Pierce, *Phys. Rev. Lett.* **67,** 140 (1991).
4. M.N. Baibich, J.M. Broto, A. Fert, F. Nguyen Van Dau, F. Petroff, P. Eitenne, G. Creuzet, A. Friederich, J. Chazelas, *Phys. Rev. Lett.* **61,** 2472 (1988).
5. G.P. Felcher, *Physica B* **192,** 137 (1993).
6. V. Lauter-Pasyuk, H.J. Lauter, B. Toperverg, O. Nikonov, E. Kravtsov, M.A. Milyaev, L. Romashev, V. Ustinov, *Physica B* **283,** 194 (2000).
7. D.L. Nagy, L. Bottyán, L. Deák, E. Szilágyi, H. Spiering, J. Dekoster, G. Langouche, *Hyp. Int.* **126,** 353 (2000).
8. D.L. Nagy, L. Bottyán, B. Croonenborghs, L. Deák, B. Degroote, J. Dekoster, H.J. Lauter, V. Lauter-Pasyuk, O. Leupold, M. Major, J. Meersschaut, O. Nikonov, A. Petrenko, R. Rüffer, H. Spiering, E. Szilágyi, *Phys. Rev. Lett.* **88,** 157202 (2002).
9. K. Temst, E. Kunnen, V.V. Moshchalkov, H. Maletta, H. Fritzsche, Y. Bruynseraede, *Physica B* **276278,** 684 (2000).
10. L. Bottyán, L. Deák, J. Dekoster, E. Kunnen, G. Langouche, J. Meersschaut, M. Major, D.L. Nagy, H.D. Rüter, E. Szilágyi, K. Temst, *J. Magn. Magn. Mater.*, **240,** 514 (2002).
11. M. Major, L. Bottyán, D.L. Nagy, Yu.V. Nikitenko, A. Petrenko, V. Proglyado, E. Szilágyi, F. Tanczikó, *this booklet*.

Formation and Ripening of Antiferromagnetic Domains in a Fe/Cr Multilayer

M. Major, L. Bottyán, D.L. Nagy, E. Szilágyi, F. Tanczikó
(KFKI Research Institute for Particle and Nuclear Physics, Budapest, Hungary)
Yu.V. Nikitenko, A. Petrenko, V. Proglyado (Frank Laboratory of Neutron Physics, JINR, Dubna, Russia)

Antiferromagnetically (AF) coupled metallic multilayers [1] are materials of great importance both from fundamental [2, 3] and application [4] point of view. In a previous study [5] part of which is also being presented [6] in this booklet, we demonstrated how off-specular polarized neutron reflectometry (PNR) [7, 8] and off-specular synchrotron Mössbauer reflectometry (SMR) [9] can be used to study a magnetic-field-history-dependent transformation of domains in a strongly AF-coupled Fe/Cr ML. More specifically we showed that, in increasing magnetic field, an explosion-like increase of the domain size by at least one order of magnitude, i.e., a *domain coarsening* takes place in an epitaxial $MgO(001)/[^{57}Fe(26Å)/Cr(13Å)]_{20}$ superlattice when the system passes the bulk-spin-flop transition at $H_{SF} = (14\pm2)$ mT. The initial state of the domain coarsening transition is the domain structure at remanence following a gradual decrease of the external magnetic saturation. In this state, the domain structure turned out to consist of relatively small domains with a correlation length $\xi = 800$ nm of the layer magnetization. Nevertheless, it remained an open question whether this state is identical with the native domain state, which is formed immediately after leaving the saturation region. We will present how PNR can be used to clarify this problem. Complementary SMR studies will be published elsewhere [10].

The sample used in this study was the same MBE-grown $MgO(001)/[^{57}Fe(26Å)/Cr(13Å)]_{20}$ superlattice, which was investigated in our previous experiments [5, 11]. The PNR experiment was performed at the REMUR polarized neutron reflectometer of the Dubna pulsed reactor IBR-2. The sample was placed between the poles of an electromagnet applying an in-plane field parallel to one easy magnetization axis of the ML and to the linear polarization of the incoming neutrons. A spin flipper before the sample could flip the polarization of the incoming neutrons. A position-sensitive detector detected the neutrons reflected by the ML so that the scattered neutrons were mapped in the q_z-q_x plane of the scattering vector **q** in two (R^+ and R^-) channels. As a rule, no spin analysis was performed. This was justified by the fact that the AF component of the layer magnetizations in this fully compensated ML was known [5,11] to align perpendicular to the external field, i.e., to the neutron spins. Accordingly, the AF reflection was expected to appear only in the R^{+-} and R^{-+} spin-flip channels, a fact subsequently verified in a few low-statistics measurements, in which spin analysis was performed with

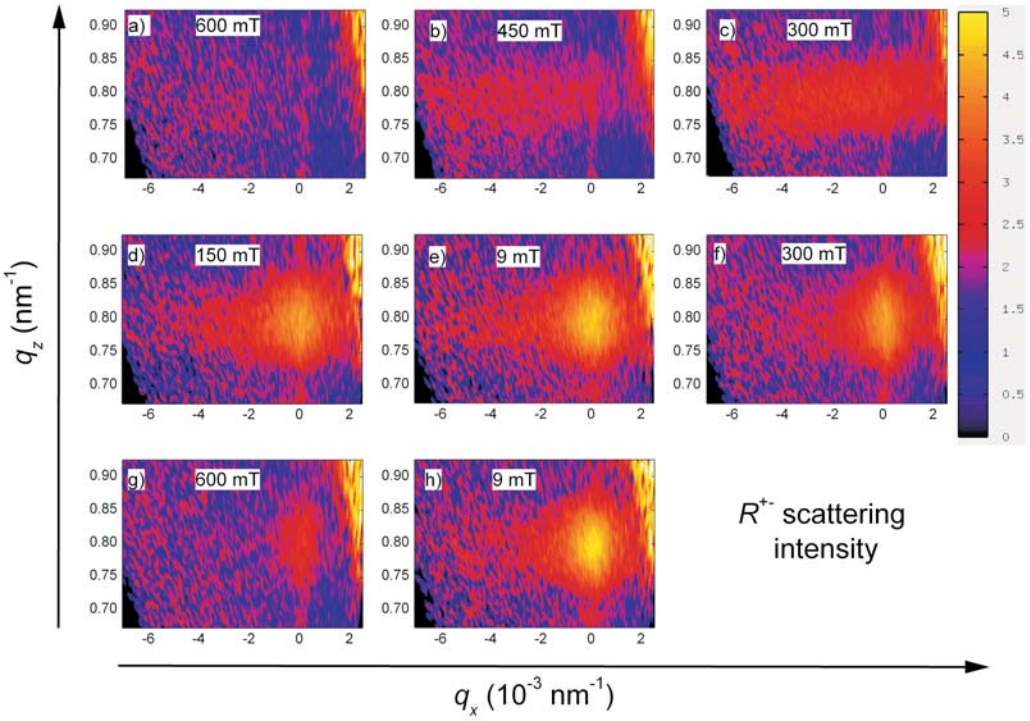

Fig.1. Domain ripening in a MgO(001)/[^{57}Fe(26Å)/Cr(13Å)]$_{20}$ multilayer as observed with PNR. The magnetic field history corresponds to saturation (not shown) a), h). Note the marked difference between patterns a) and g) as well as between patterns c) and f) showing the irreversible character of domain ripening.

the insertion of an additional spin flipper and a Soller-type supermirror stack. All measurements were performed in static magnetic fields at (286±2) K.

First the sample was saturated in 1.7 T for one minute. Afterwards, the field was decreased to 600 mT at which value the first measurement was completed. Further experiments were performed in 450 mT, 300 mT, 150 mT, at remanence (9 mT), again in 300 mT, 600 mT and, finally, in 9 mT. Fig. 1 a) to h) show the $R^{+} = R^{+-}$ scattering intensity around the AF reflection ($q_z = 0.80$ nm^{-1}).

The AF reflection always consists of a broad diffuse sheet. However, besides the expected field dependence of the total AF reflection intensity, also a marked change in the width and shape of the diffuse sheet is observed, which is taking place between 300 mT and remanence in fields decreasing from saturation. Before the transition (Fig. 1 a) to c)), the domain size as calculated from the width of the diffuse sheet ($\xi = 1/\Delta q_x$) is $\xi = 370$ nm, a value increasing to $\xi = 800$ nm after the transition (Fig. 1 e)). The transition that we shall call, henceforth, *domain ripening*, proves to be irreversible (Fig. 1 f) to h)). Furthermore, ripening is associated with a characteristic change of the shape of the layer magnetization autocorrelation function [10].

The main features of the ripening process may be qualitatively well understood in terms of a simple phenomenological model. Starting in magnetic saturation and then gradually decreasing the field, two kinds of AF domains differing only in the sense of rotation of the magnetization in their odd and even layers are spontaneously formed. The size of the native domains is determined by the ratio of the bulk and the interlayer exchange couplings,

its typical value being a few 100 nm. On further decreasing the field and, provided that the native domain size is small enough, the size of the domains is expected to spontaneously increase in order to decrease the domain-wall energy per unit area of the ML. The increase of the domain size is associated with the movement of the domain walls, a dissipative, 'friction'- (coercivity-) limited process (domain-wall pinning). The domain-wall density is decreasing with increasing domain size and, at low enough external magnetic field, there will be not enough driving force available for further increasing the domain size. Therefore ripening starts at a certain decreasing field and stops at another (lower) decreasing field. Obviously, the described scenario results in an irreversible behavior. The two critical fields of ripening lie, according to the present PNR results, between 350 and 9 mT for the sample studied (actually at 200 and 100 mT), according to SMR experiments [10].

In conclusion, we observed for the first time *domain ripening*, the spontaneous and irreversible, domain-wall-energy-driven and coercivity-limited increase of the size of native domains in a strongly AF-coupled Fe/Cr superlattice in decreasing external magnetic field.

References:

1. P. Grünberg, R. Schreiber, Y. Pang, M.B. Brodsky, H. Sowers, *Phys. Rev. Lett.* **57,** 2242 (1986).
2. S.S.P. Parkin, N. More, K.P. Roche, *Phys. Rev. Lett.* **64,** 2304 (1990).
3. J. Unguris, R.J. Celotta, D.T. Pierce, *Phys. Rev. Lett.* **67,** 140 (1991).
4. M.N. Baibich, J.M. Broto, A. Fert, F. Nguyen Van Dau, F. Petroff, P. Eitenne, G. Creuzet, A. Friederich, J. Chazelas, *Phys. Rev. Lett.* **61,** 2472 (1988).
5. D.L. Nagy, L. Bottyán, B. Croonenborghs, L. Deák, B. Degroote, J. Dekoster, H.J. Lauter, V. Lauter-Pasyuk, O. Leupold, M. Major, J. Meersschaut, O. Nikonov, A. Petrenko, R. Rüffer, H. Spiering, E. Szilágyi, *Phys. Rev. Lett.* **88,** 157202 (2002).
6. D.L. Nagy, L. Bottyán, L. Deák, J. Dekoster, H.J. Lauter, V. Lauter-Pasyuk, M. Major, O. Nikonov, A. Petrenko, E. Szilágyi, *this booklet*.
7. G.P. Felcher, *Physica B* **192,** 137 (1993).
8. V. Lauter-Pasyuk, H.J. Lauter, B. Toperverg, O. Nikonov, E. Kravtsov, M.A. Milyaev, L. Romashev, V. Ustinov, *Physica B* **283,** 194 (2000).
9. D.L. Nagy, L. Bottyán, L. Deák, E. Szilágyi, H. Spiering, J. Dekoster, G. Langouche, *Hyp. Int.* **126,** 353 (2000).
10. M. Major, D. Aernout, L. Bottyán, A. Chumakov, B. Croonenborghs, L. Deák, B. Degroote, J. Dekoster, O. Leupold, J. Meersschaut, D. L. Nagy, R. Rüffer, J. Swerts, E. Szilágyi, F. Tanczikó, K. Temst, V. Vanhoof, A. Vantomme, *to be published*.
11. L. Bottyán, L. Deák, J. Dekoster, E. Kunnen, G. Langouche, J. Meersschaut, M. Major, D.L. Nagy, H.D. Rüter, E. Szilágyi, K. Temst, *J. Magn. Magn. Mater.*, **240,** 514 (2002).

Simulations of off-Specular Polarized Neutron and Synchrotron Mössbauer Reflectometry

Yu. N. Khaidukov (Frank Laboratory of Neutron Physics, JINR, Dubna, Russia)
L. Deák, D.L. Nagy, L. Bottyán (KFKI Research Institute for Particle and Nuclear Physics, Budapest, Hungary)
H. Spiering (Institut für Anorganische und Analytische Chemie, Johannes Gutenberg Universität, Mainz,Germany)

The chemical, the magnetic or isotopic composition of a thin homogeneous film or a stratified structure can be suitably studied by reflectometric techniques and they are manifested in the one-dimensional scattering amplitude density depth profile within the penetration depth of the corresponding radiation. Specular X-ray and neutron reflectometry, therefore, have become standard tools in studying surfaces and thin films.

If the alignment of the surface parameters is of importance, a study by polarized radiation is necessary. In the most important cases the scattering medium is birefringent for the corresponding radiation, and the polarization-dependent multiple scattering leads to non-scalar optics. These cases include polarized neutron reflectometry (PNR) and (synchrotron) Mössbauer reflectometry (SMR).

Due to the magnetization sensitivity of PNR, the depth profile of the neutron scattering amplitude reflects the depth profile of magnetization in the stratified medium. Therefore the full magnetization depth profile can be deduced from PNR experiments performed with spin analysis of the scattered neutrons. SMR, the grazing-incidence nuclear resonant scattering of synchrotron radiation is a special but well-studied case of the anisotropic (resonant) x-ray scattering problem.

Time-differential (TD) SMR contains the hyperfine interaction (i.e., magnetization) information in the quantum beats of the time response that follows the excitation of the system by the synchrotron radiation pulse at one or at a series of different grazing angles. In a time-integral (TI) SMR experiment all delayed (i.e., nuclear resonantly scattered) photons are counted as a function of the grazing angle. This method is very similar to PNR and yields integral hyperfine depth profile and superstructure information.

The evaluation of the *specular* SMR spectra is based on the concept of 4x4 characteristic matrices [1], a method equivalent to the supermatrix method [2], which was later developed for specular PNR. A common optical description exists and was formulated for the anisotropic neutron and anisotropic nuclear resonant x-ray reflection [3], allowing for a very efficient numerical algorithm for both SMR and PNR. The corresponding computer program EFFI (Environment For FItting) is readily available for *specular* reflectometry of layered systems of arbitrary complexity [4,5]. EFFI is capable for *simultaneous* fitting spectra of different types. As an example, simultaneous fits of non-

resonant x-ray, PNR and SMR spectra of an isotope-periodic $^{57}Fe/^{56}Fe$ multilayer (ML) is shown in Fig. 1.

The specularly reflected radiation from a stratified system depends on the lateral averages of the material parameters and it is insensitive to the *lateral structure* of the film. For studying lateral inhomogeneities, such as structural roughness, magnetic domains, etc., *off-specular* reflectometry has to be used. Domain structure of antiferromagnetically (AF) coupled MLs is an issue of both theoretical and technological importance. With the advent of two-dimensional position sensitive detectors, time-of-flight neutron installations are capable of making maximum use of the scattered intensity and record the intensity in a certain scattering angle and wavelength range simultaneously. Due to the extreme time resolution requirements, avalanche photodiode arrays are not yet available at present for multidimensional detection of off-specular SMR spectra, ω-scans at various 2θ scattering angles are measured instead.

A theory of the off-specular neutron reflectometry using the Distorted-Wave Born Approximation (DWBA) has been published earlier [2,6]. The idea to apply the DWBA technique to describe off-specular SMR experiments is therefore obvious. However, due to the temporal character of SMR, this approach was not straightforward. Starting from Lax' general theory [7] and from the common optical formalism of PNR and SMR [3], an expression for diffuse scattering of electromagnetic and/or quantum mechanical particle waves on laterally inhomogeneous stratified media

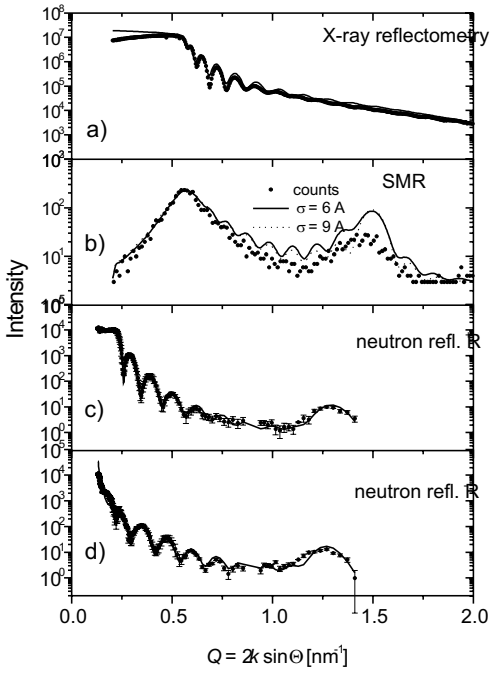

Fig.1. Different types of reflectometric measurements of a $[^{57}Fe(2.33\ nm)/^{nat}Fe(2.33\ nm)]_{10}$ multilayer. The data evaluation was made in terms of the common optical algorithm (see text), using the computer program EFFI.

was recently obtained, and the off-specularly reflected intensity was expressed in terms of the geometrical correlation functions of the lateral structure (inhomogeneity) and the specular field profile in the layers [8].

This new common off-specular theory has been recently implemented in the evaluation program EFFI. The complexity of the problem requires the optimization of handling the large amount of PNR and SMR data as well as the organization and handling the various ML parameters in a manner that maintains generality on one hand and practical treatment of very different ML structures on the other, on computers accessible at present. Consequently, a number of new algorithms have to be built in EFFI.

As first step, an independent simulation program was written to calculate off-specular SMR and PNR spectra. Those of an $[^{57}Fe(2.6\ nm)/Cr(1.3\ nm)]_{20}$ antiferromagnetic ML were calculated

and compared, to check the efficiency of the current algorithms [8].
Another example for the application is shown in Fig. 2, where the two-dimensional neutron reflectivity data (left panel) and theoretical simulations (right panel) for an $[^{57}Fe(3nm)/V(2.1nm)]_{20}/MgO(001)$ ML sample are compared as function of outgoing angle Θ_2 and wavelength λ of the neutrons. The experiment was conducted on REMUR, the new polarized neutron reflectometer at the IBR-2 reactor [9]. The correlation length of ξ~400nm was attributed to structural in homogeneities rather than an average in-plane antiferromagnetic domain size, since the applied 440 mT external field ensured single domain structure of the ML sample.

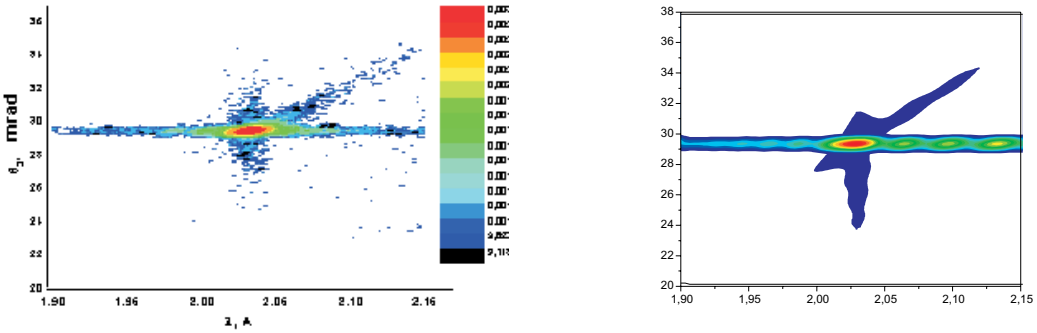

Fig.2. Experimental (left) and theoretical (right) neutron intensity maps for $[^{57}Fe(3nm)/V(2.1nm)]_{20}/MgO(001)$ multilayer sample as a function of outgoing angle θ_2 and wavelength λ of the neutrons. The incident angle of the neutrons and the external magnetic field were θ_1=29.4 mrad, and H=440 mT, respectively.

References:

[1] L. Deák, L. Bottyán, D.L. Nagy, H. Spiering, Phys. Rev. B 53 (1996) 6158.
[2] A. Rühm, B.T. Toperverg, H. Dosch, Phys. Rev. B 60 (1999) 16073.
[3] L. Deák, L. Bottyán, D.L. Nagy, H. Spiering, Physica B 297 (2001) 113.
[4] H. Spiering, L. Deák, and L. Bottyán, Hyp. Int. 125 (2000) 197.
[5] The computer program EFFI is available from ftp://iacgu7.chemie.uni-mainz.de/pub/effi
[6] B.T. Toperverg, Physica B 297 (2001) 160.
[7] M. Lax, Rev. Mod. Phys. 23 (1951) 287.
[8] L. Deák, L. Bottyán, D.L. Nagy, H. Spiering, Yu.N. Khaidukov, submitted to Phys. Rev. B.
[9] V.L. Aksenov, V.V .Lauter-Pasyuk, H. Lauter, Yu.V.Nikitenko, A.V. Petrenko, Physica B 335 (2003) 147. V.L. Aksenov, K.N. Jernenkov, S.V. Kozhevnikov, H. Lauter, V. Lauter-Pasyuk, Yu.V. Nikitenko, A.V. Petrenko, JINR Communications, D13-2004-47, Dubna, 2004.

Structural Studies of Ferrofluids by Small-Angle Neutron Scattering

M.V.Avdeev, M.Balasoiu, V.L.Aksenov (Frank Laboratory of Neutron Physics, JINR, Dubna, Russia)
Gy.Török, L.Rosta (KFKI Research Institute for Solid State Physics and Optics, Budapest, Hungary)
D.Bica, L.Vékás (Center for Fundamental and Advanced Technical Research, Timisoara, Romania)

Dispersions of magnetic materials stabilized by adding surfactants are known since 1960s as ferrofluids (magnetic fluids). Due to specific properties in a magnetic field they are actively used in different industrial, technical, as well as in biological and medical applications. Typical ferrofluid is a colloidal solution of magnetic particles (magnetite, cobalt, e.c.) covered by either neutral or charged surfactant shell in a liquid carrier (Fig.1). Relationship between characteristic size of the particles and interparticle interaction, especially under the external magnetic field, determines the stability of the fluids in respect to sedimentation and coagulation. The knowledge about the microstructure of ferrofluids is very important to understand and control the mechanisms of their stabilization.

Neutron scattering methods have been largely used during last two decades for determining structural characteristics of magnetic fluids at microscopic level including structure and interaction of colloidal particles,

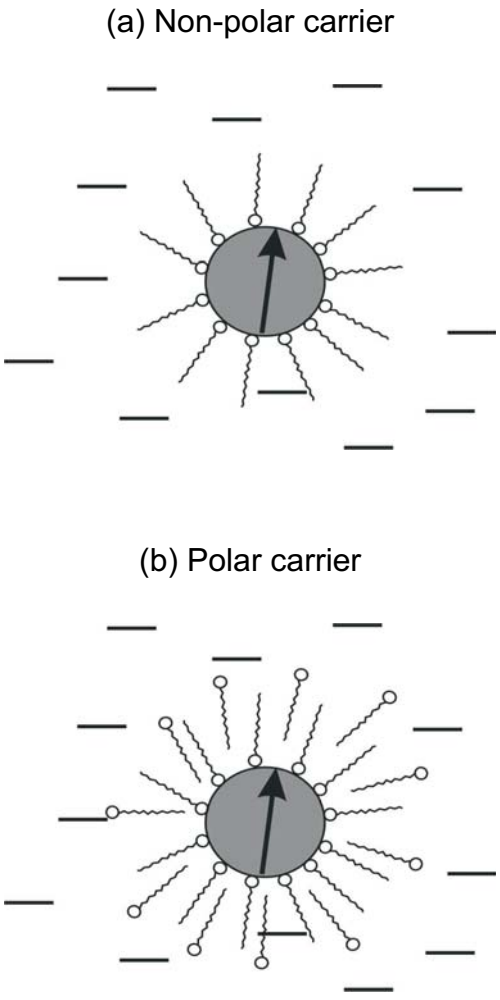

Fig.1. Schematic view of the structure for ferrofluids based on non-polar (a) and polar (b) carriers. The surfactant layer avoids the coagulation of the interacting particles. In contrast to non-polar ferrofluids with single surfactant layer around magnetic particles (chemiosorption) The double layered stabilization (b) is achieved by the excess of free surfactant in the system followed by the physical absorption of surfactant on the first layer around magnetite particles.

aggregation phenomena, the magnetic hydrodynamics. Small-angle neutron scattering (SANS) is the effective method to study the structure of ferrofluids under a wide variety of experimental conditions. Examples of the SANS curves for different ferrofluids and their interpretation are given in Figs.2, 3. The curves were obtained at the small-angle diffractometers YuMO (FLNP, JINR, Dubna) and "Yellow Submarine" (RISSPO, Budapest).

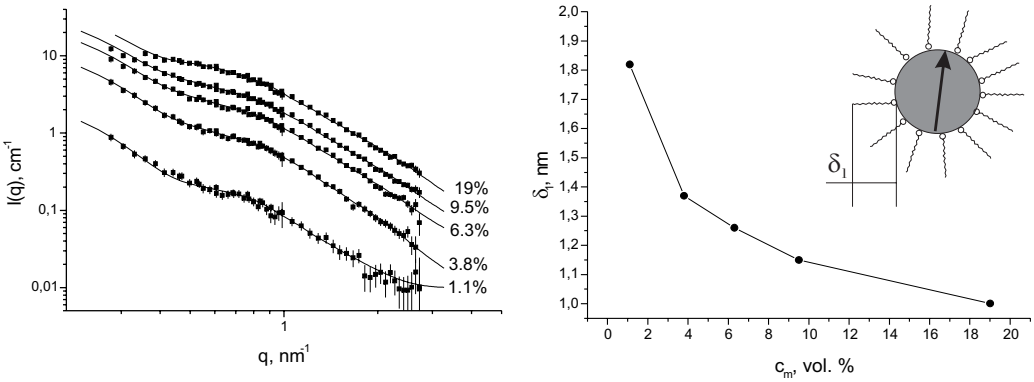

Fig.2. Experimental (points) and model (lines) SANS curves obtained for the system magnetite/oleic acid/benzene at different volume fraction of magnetite indicated to the right. The core-shell model fits well the experimental data. The change of the surfactant (oleic acid) layer thickness (δ_1) with the growth of the particle concentration is revealed. This points to the fact that the interparticle interaction increasing with the concentration presses the surfactant tails in the layer closer against the magnetite surface. Despite the fact that the magnetic scattering in the system was not taken into account, the model curves fit well to experimental ones, which points to a small effect of the magnetic scattering in the studied systems.

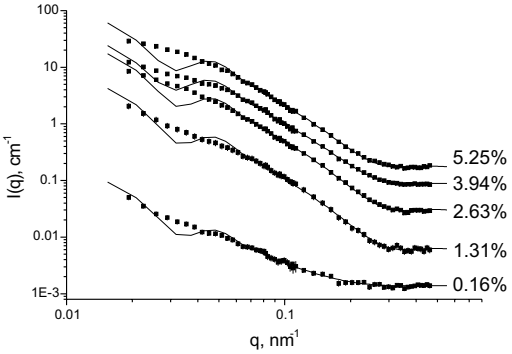

Fig.3. Experimental (points) and model (lines) SANS curves obtained for the system magnetite/double layer of dodecylbenzenesulphonic acid/water at different volume fraction of magnetite indicated to the right. The core-shell model does not fit well the experimental curves, which points to the complex structure of the ferrofluids. Possible reasons for large deviation from the standard model are the formation of stable aggregates in initial samples, the appearance of micelles of free surfactants, as well as specific strong interaction between particles.

References:

M.V.Avdeev, M.Balasoiu, D.Bica, L.Rosta, Gy.Török, L.Vékás *Materials Science Forum* 373-376 (2001) 457
M.Avdeev, M.Balasoiu, Gy.Török, D.Bica, L.Rosta, V.L.Aksenov, L.Vékás, *J. Mag. Mag. Mater.* 252 (2002) 86
V.Aksenov, M.Avdeev, M.Balasoiu, L.Rosta, Gy.Török, L.Vékás, D.Bica, V.Garamus, J.Kohlbrecher, *Appl. Phys. A*, 74 (2002) s943
V.L.Aksenov, M.V.Avdeev, M.Balasoiu, D.Bica, L.Rosta, Gy.Török, L.Vékás, *J. Mag. Mag. Mater.*, 258-259 (2003) 452
D.Bica, L.Vékás, M.V.Avdeev, M.Balasoiu, O.Marinicã, F.D. Stoian, D.Susan-Resiga, Gy.Török, L.Rosta, *Prog. Colloids Polymer Sci.* 125 (2004) 1

Cluster state of fullerene in solutions. Data of small-angle neutron scattering.

M.V.Avdeev, T.V.Tropin, V.L.Aksenov (Frank Laboratory of Neutron Physics, JINR, Dubna, Russia)
A.A.Khokhryakov (Kyiv Taras Shevchenko National University, Ukraine)
G.V.Andrievsky (Institute for Therapy of Ukrainian AMS, Kharkov, Ukraine)
V.B.Priezzhev (Bogoliubov Laboratory of Theoretical Physics, JINR, Dubna, Russia)
M.V.Korobov (Lomonosov Moscow State University, Moscow, Russia)
L.Rosta (KFKI Research Institute for Solid State Physics and Optics, Budapest, Hungary)

Fullerenes (Fig.1), unlike other allotropic forms of carbon, graphite and diamond, dissolve well in different organic solvents. The use of this property in fullerene production, as well as some other (e.g. medical) applications, arouses a great interest in the study of fullerene solutions. Very often fullerene solutions have specific properties, such as non-monotonous solubility behavior with respect to temperature and solvatochromism (sharp change in the absorption spectrum with a slight change in the content of the solvent). One of the discussed reasons for this is the formation of fullerene clusters in the solutions.

Highly stable and reproducible colloidal water solutions of C_{60} fullerenes (FWS) obtained [1] by transferring fullerenes from an organic solution into an aqueous phase with the help of ultrasonic treatment have been investigated by means of small-angle neutron scattering (SANS) [2]. SANS curves were obtained at the small-angle diffractometers of the Budapest Neutron Center and Frank Laboratory of Neutron Physics (JINR, Dubna). A polydispersity in the size of detected particles up to 84 nm has been revealed (Fig.2). These particles are slightly anisotropic and have the characteristic size of about 70 nm. Along with it, there are some indications that a

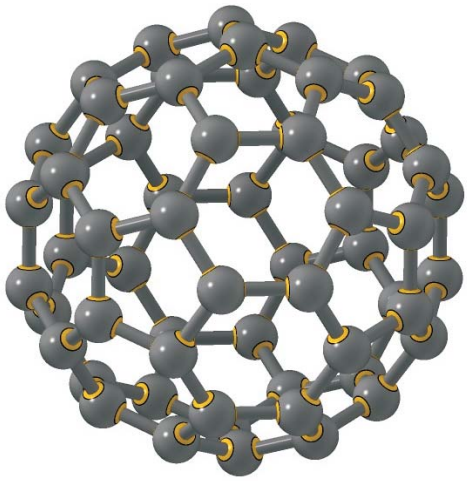

Fig.1. Atomic structure of buckminster fullerene, C_{60}.

significant part of fullerenes composes particles with the size of the order of 1 nm. The contrast variation based on mixtures of light and heavy water shows that the mean scattering length density of the particles is close to that of the packed fullerene associates, as well as that the characteristic size of possible fluctuations of the scattering length density within the particles does not exceed 2 nm. A smooth surface resulting in the Porod law for the scattering has been detected. Taking into account the data of complementary techniques (UV-Vis, IR, EM, DLS, DSC) three models to describe the particle structure can be considered [2]. The first model implies that the particles are fullerene crystallites or rather dense clusters covered with charged thin shells of hydration water, which stabilizes the solutions. According to the SANS data, in this case the fraction of the hydration shell in the particles must not exceed 5 vol. %. The second model suggests that the particles represent associates of single hydrated C_{60} fullerenes. In this case hydration water must be localized on the fullerene surface. For the suggested hydration shell of 24 water molecules the minimum possible packing density of the complexes in the particles is 0.64. The last model intended to explain an additional peak in the DSC traces different from a water peak considers the particles in FWS as closed film-like structures with water captured inside. The estimated size of such inclusion is of the same order as the particle size revealed by SANS. To satisfy SANS data, a free exchange of the captured and bulk water must take place.

In the frame of the study of stabilizing mechanizms of aqueous

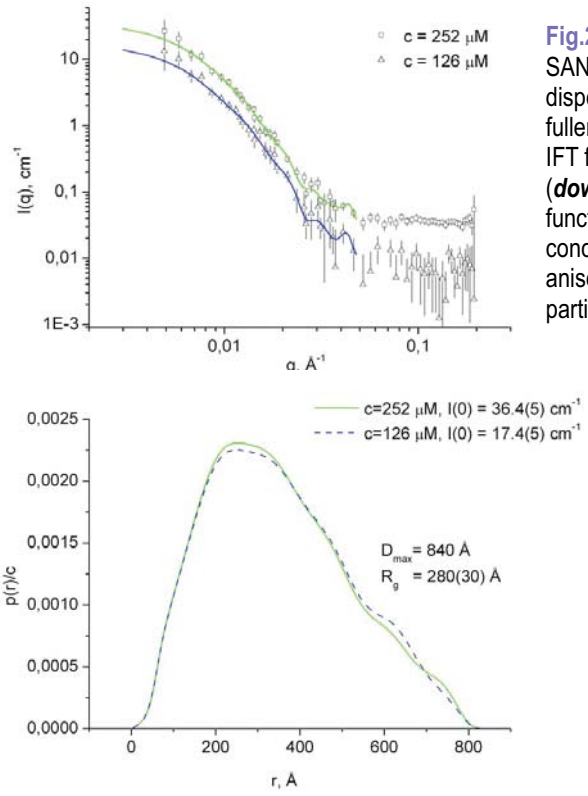

Fig.2. (***top***) Experimental SANS curves (BNC) from the dispersions with different fullerene concentrations and IFT fitting of experimental data; (***down***) Resulting *p*(*r*) functions normalized on the concentration. Slight anisotropy in the shape of the particles can be seen.

fullerene dispersions a series of solutions of C_{60} fullerene in nitrogenated solvents (n-methyl-pyralidon, benzonitrile, aniline, triethylamine) have been investigated [3]. The UV-Vis spectroscopy, dynamic light scattering (DLS) and small-angle neutron scattering (SANS) were applied to reveal the existence of clusters and their characteristic size in the solutions. Right after dilution of fullerene some of the studied systems show the formation of clusters and their growth up to the size of more than 200 nm. The effect of water addition is studied for the solution C_{60}/n-methyl-pyralidon (Fig.3). Its behaviour is close to that observed previously [4, 5] for the system C_{60}/pyridine, where the addition of water results in a significant increase in the number of clusters with characteristic size within 20-40 nm.

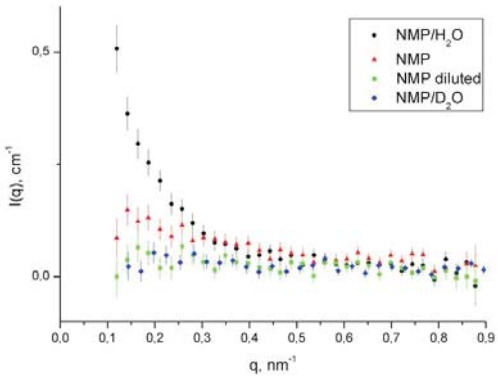

Fig.3. Scattering curves from different NMP solutions of C60 fullerene. Despite a small SANS signal in pure NMP one can conclude that quite large clusters (size more than 100 nm) were present in the solutions. The signal decreases with the decrease in the fullerene concentration. the SANS signal increases significantly when the NMP solutions are mixed with water, which reveals an appearance of clusters with the characteristic size of about 25 nm in the mixture. If the NMP solution is mixed with deuterated water the SANS signal disappears. This means that the mean scattering length densities of the clusters and the solvent in this case are close, which, in turn, points to comparatively small NMP content in the clusters.

References:

1. G.V.Andrievsky, M.V.Kosevich, O.M.Vovk, V.S.Shelkovsky, L.A.Vashchenko, *J. Chem. Soc., Chem. Commun.* **1995**, *12*, 1281-1282.
2. M.V.Avdeev, A.A.Khokhryakov, T.V.Tropin, G.V.Andrievsky, V.K.Klochkov, L.I.Derevyanchenko, L.Rosta, V.M.Garamus, V.B.Priezzhev, M.V.Korobov, V.L.Aksenov, *Langmuir*, *20* (2004) 4363
3. M.V.Korobov, M.V.Avdeev, N.V.Kozhemyakina, T.V.Tropin, A.A.Khokhryakov, L.Rosta, V.Aksenov, *In book of abstracts of the EMRS Spring Meeting, 2004. Strasbourg, May 24-28*.
4. V.L.Aksenov, M.V.Avdeev, D.Mihailovic, A.Mrzel, V.D.Vasiliev, A.A.Timchenko, I.N.Serdyuk, In *Electronic properties of novel materials molecular nanostructures*, Eds. Kuzmany, H.; Fink, J.; Mehring, M.; Roth, A. AIP Conference Proceedings, 2001.
5. V.L.Aksenov, M.V.Avdeev, A.A.Timchenko, I.N.Serdyuk, R.P.May, In *Frontiers of Multifunctional Nanosystems*, Eds. Buzaneva, E.; Scharff, P. Kluewer Academic Publishers: Netherlands, 2002.

SANS Study of Colloidal Aggregates of Silicon Tetraethoxide in Basic Ethanol/Water Solutions

M.V.Avdeev, V.L.Aksenov (Frank Laboratory of Neutron Physics, JINR, Dubna, Russia)
J. Kohlbrecher (Paul Scherrer Institute, Villigen, Switzerland)
L.Rosta (KFKI Research Institute for Solid State Physics and Optics, Budapest, Hungary)

Data of small-angle neutron scattering from colloidal aggregates of silicon tetraethoxide (TEOS) in basic ethanol/water solutions are presented [1]. Changes in the structure of the aggregates were followed for different H_2O:TEOS molar ratio (w) within the interval from 0.5 to 10. Two scattering levels are detected. The first one (< 10 nm) corresponds to the diffusive surface of the aggregates whose characteristics change with w-ratio. The second level reflects the formation of large secondary associations, which have a fractal dimension decreasing monotonously from 2.2 to 1.0 with increasing w-ratio.

The study of the growth of branched polymeric compounds is of current interest. One of the materials most widely used to produce branched polymers is silicon tetraethoxide (TEOS). After hydrolysis it forms aggregates, which results in a wide class of different structures depending on the H_2O:TEOS ratio *(w)* and on other parameters (pH, temperature, total concentration) as well.

The studied samples were prepared according to the procedure described in Ref.2. Water was added with different proportions to the 10% TEOS (Fluka) ethanol solution so that the H_2O:TEOS molar ratio was changed from 0.5 to 10 (11 points in a w-interval 0.5÷2 and several points for $w > 2$). The hydrolysis was base-catalyzed (0.01 M NH_4OH). During the period between the preparation and SANS experiments (about seven days) samples were kept at 20°C (despite one day during the transportation). Sample preparation and experiments on small-angle neutron scattering were performed twice at the SANS diffractometers of the Budapest Neutron Center (Hungary) and of the Paul Scherrer Institute (Switzerland) and showed complete reproducibility.

Scattering patterns for several w-ratio values obtained are presented in Fig.1. Two distinct regions are observed in the double logarithmic plot, which can be interpreted as mass and surface

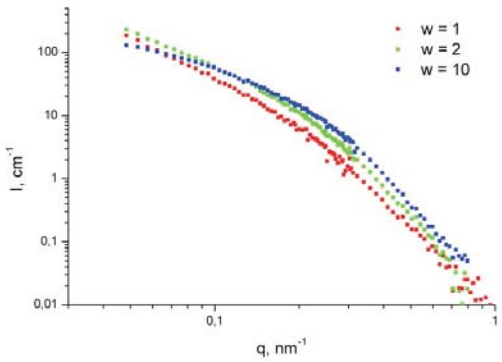

Fig.1. Scattering curves for several *w*-ratio values.

scattering [3], respectively. To treat the data we used the unified exponential/power-law approach [4] for two scales:

$$I(q) = G\exp(-q^2R^2/3) + B\exp(-q^2R_s^2/3)\,(1/q^*)^P + G_s\exp(-q^2R_s^2/3) + B_s\,(1/q_s^*)^{Ps}, \quad (1)$$

where R is the radius of gyration; P is the exponent of the power law (slope in the log-log plot), which determines [3] whether your system is mass fractal ($P < 3$), surface fractal ($3 < P < 4$) or possesses a so-called diffusion surface ($P > 4$); G and B are the parameters comprising information about the concentration and volume of the particles, as well as their contrast against the solvent; and $q^* = q/[\mathrm{erf}(qkR/6^{1/2})]^3$. Parameters without index and with the s index correspond to the mass (first scale) and surface (second scale) scattering, respectively. The constant k in the expression for q^* is empirical and equals to 1.6 and 1.0 for the mass and surface scale, respectively. The fitting procedure is illustrated in Fig.2.

Resulting parameters as a function of the w-ratio are presented in Figs. 3, 4. The ratio G_s/R_s^6 (Fig.4) is proportional to the product of the total concentration of the subunits in solution by their contrast. One can see that homogeneous aggregates with the diffusive surface (P_s>4) in contrast to the previous study [4], (P_s<4), are detected. The significant difference is not clear for the moment. Nevertheless, we should note that both experiments result in the fact that the w-ratio of about 2 is a critical one in the sense that the w-dependence of parameters of aggregates (P_s, R_s, G_s) has a peculiarity in the vicinity of 2. In the data presented here (Figs.3, 4) the

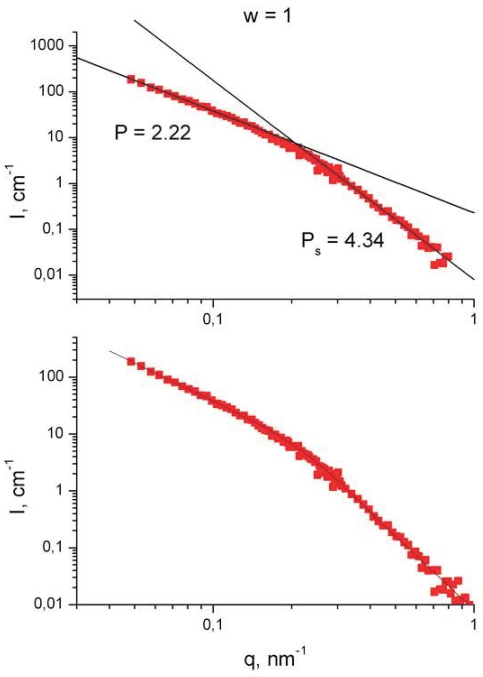

Fig.2. Experimental and model curves for w=1. Resulting parameters are B=0.23(1), P=2.22(2), B_s=0.0081(4), P_s=4.34(5), G_s=12.6(7), R_s=9.3(1).

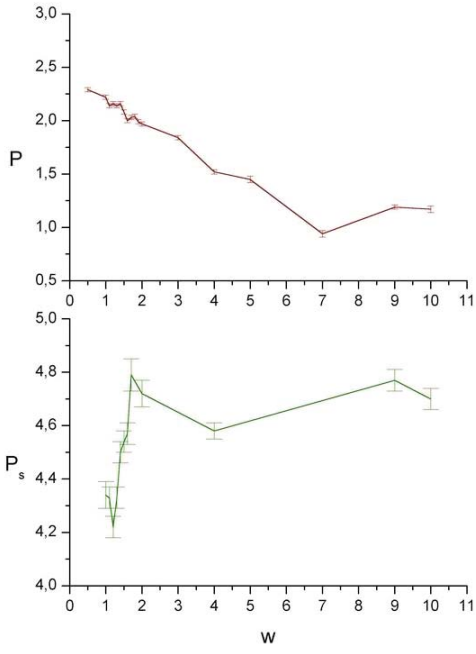

Fig.3. Exponents P, P_s obtained from the fits as a function of the w-ratio.

character of the surface (parameter P_s) changes significantly with the w-ratio below 2, as well as the radius of aggregates (R_s) increases from 9 to 10 nm. For the w-ratio above 2 the surface of subunits does not change much, while the radius R_s decreases from 10 to 7 nm. This indicates that the effect of "poisoned bonds" [4] (when OH groups get to the aggregates and are not hydrolyzed) is insignificant for w > 2. An interesting observation of the current work is that the considered aggregates, in their turn, are the subunits of the bigger associations with characteristic size more than at least 100 nm. It seems that their formation should be an additional factor affecting the growth of subunits, and vice versa. Nevertheless, in contrast to the parameters of the subunits, the fractal dimension of the associations, $D=P$, does not show any peculiarity in the studied w-interval (Fig.2) and decreases monotonously from 2.2 to 1.0 with increasing w-ratio. Thus the growth processes of the associations and subunits are somewhat independent. In summary, TEOS solutions testify the variation and complexity of the possible structures during the hydrolysis. In conjunction, the behavior of the systems as a function of the w-ratio may be considered as critical at w-values in a vicinity of 2. SANS is a proper technique to investigate such systems in a scale range 1-100 nm, and we hope that the next studies based on the contrast variation with hydrogen/deuterium substitution could clarify the inner structure of the aggregates.

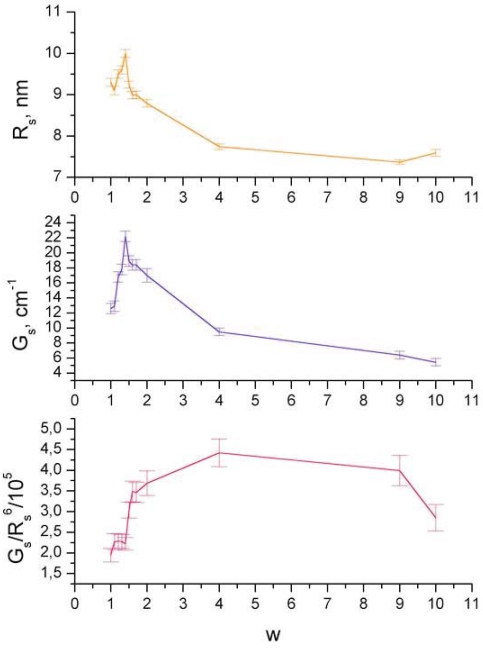

Fig.4. Fit results for radius of gyration of subunits R_s, parameter G_s and the ratio G_s / R_s^6 as a function of the w-ratio.

References:

[1] M.V.Avdeev, V.L.Aksenov, J. Kohlbrecher, L.Rosta, Physica B (2004), in press.
[2] K.D.Keefer & D.W.Schaefer, Phys. Rev. Lett. 56 (1986) 2376.
[3] P.W.Schmidt, in: Modern Aspects of Small-angle Scattering, ed. H.Brumberger (Kluwer Academic Publishers, Netherlands, 1995) p.1.
[4] G.Beaucage, J. Appl. Cryst. 29 (1996) 134.

Structure of Aqueous Solutions of 2-Butoxyethanol by Small-Angle Neutron Scattering and Kirkwood-Buff Integrals

L.Almásy (KFKI Research Institute for Solid State Physics and Optics, Budapest, Hungary)
A.K.Islamov, A.I.Kuklin (Frank Laboratory of Neutron Physics, JINR, Dubna, Russia)

Many binary and ternary liquid mixtures exhibit pronounced deviations from the ideal mixing, which are reflected, for example, in the miscibility behaviour of the two components in the phase space, and in forming different types of aggregated structures. The deviation from the ideal (random) mixing is caused by the intermolecular forces, which are usually of short-range character, and sometimes directional, like hydrogen bonding. The combination of all these effects leads to a great variety of the forms of structures in different mixtures.

The statistical thermodynamics provides a route to describe the structure of a liquid mixture in terms of a few thermodynamic, measurable quantities, such as the compressibility, the density, and the free energy of mixing. Using these data, the Kirkwood-Buff formalism allows one to calculate structural characteristics of the mixture, the so-called Kirkwood-Buff integrals (KBIs), which are the integrals of the partial pair correlation functions over the whole space. Interestingly, they can be computed from the three mentioned quantities, or, alternatively, using the compressibility, the density and the zero-angle limit of the total structure factor, which can be measured by small-angle X-ray or neutron scattering. The knowledge of the Kirkwood-Buff integrals for a binary mixture over the whole composition range provides a useful tool to characterize the interactions between the species, in terms of preferential attraction or repulsion between species, and clustering. They have been calculated from thermodynamic data for a large amount of binary systems, mostly aqueous solutions, by several authors [1,2,3]. These compilations have shown that the precision of such obtained KBIs is very often limited by the low quality of the free energy of mixing data, obtained usually from vapor pressure measurements. Recent works demonstrated that in many cases, the use of the forward scattering intensity instead of the free energy of mixing can substantially improve the precision of the KBIs, numerically their precision can be made equal to the precision of the experimental forward scattering, which falls in the range of 1 - 5 % when using X-ray or neutron scattering. Therefore, an important task for the future is to recalculate the KBIs for the most interesting systems, using data from scattering experiments. In addition, the small-angle scattering measurements provide additional information on the structure of the mixtures, namely the size and form of the aggregates in solutions, if they are of the order of 1-100 nanometers, i.e. typical range for surfactant solutions, the structure of which is interesting by its own.

In the present work we studied the behavior of the aqueous solution of a typical nonionic surfactant, 2-butoxyethanol (BE) :

CH_3-CH_2-CH_2-CH_2 - O - Ch_2 - CH_2 - OH

It was known from previous works, that in the concentration range 2 - 10 mol% they form micelle-like aggregates, and that the solution is demixing into two phases increasing the temperature above 43°C. The presence of spherical micelle-like aggregates was assumed on the basis of SANS [4] and light scattering experiments, but no evidence in the sphericity was obtained in those studies. The Kirkwood-Buff integrals for this system were calculated by several authors, and the results were unfortunately in a strong disagreement with each other. In our work, we tried to characterize the 2-butoxyethanol solutions using SANS and the Kirkwood - Buff approach.

The experiments have been performed on the time-of-flight SANS spectrometer "YuMO", in Dubna. Mixtures with 2-butoxyethanol mole fractions between 0.03 and 0.15 were measured at temperatures 15, 25 and 35°C. The spectra for one of them are shown in the Figure 1. The increase of the scattering intensity with increasing temperature is due to the more pronounced concentration fluctuations, which lead to demixing to a water-rich and a solute-rich phase above 43°C. The form of the scattering curves can be well described by the Ornstein-Zernike model of concentration fluctuations, the formula and the fitted lines are shown in the Figure 1.

The results for all samples at all concentrations are shown in Figure 2, a,b. Long range correlations in the composition are observed in the mixtures, having maximum at about 0.05 mole fraction of BE. The behavior of the intensities and the correlation lengths are characteristic for binary mixtures in state close to phase separation. The form of the scattering curves allows one to construct simple and more complicated models. The simplest possibility is that the

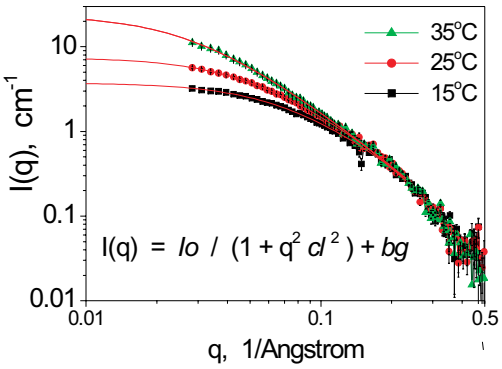

Fig.1. SANS spectra of 3 mol% solutions of 2-butoxyethanol in heavy water.

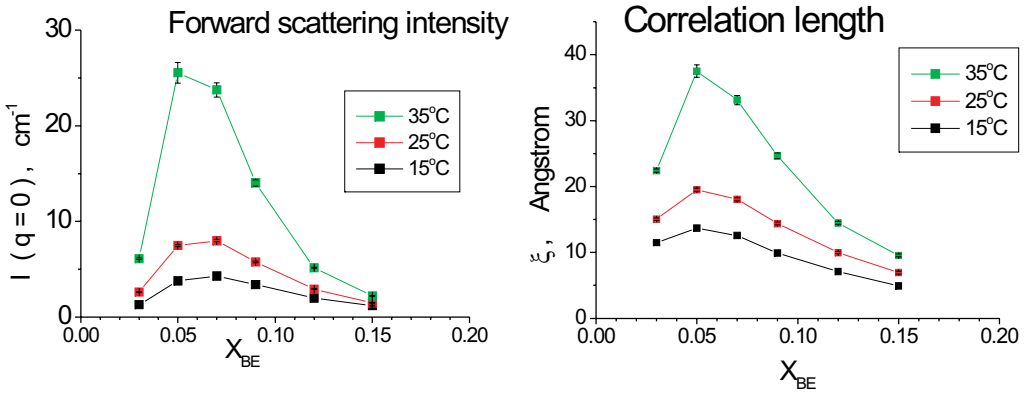

Fig.2. Forward scattering intensities (a) and correlation lengths (b) of concentration fluctuations, obtained from fitting the model equation to the SANS spectra.

butoxyethanol molecules arrange themselves in a loose network, so that their spatial distribution perfectly resembles the distribution of molecules in a two-component mixture with statistical concentration fluctuations. More elaborated models of interacting spherical micelles were used in earlier studies [4], which led to conclusions similar to ours, namely that loose objects are formed in the mixtures consisting of aggregated water and butoxyethanol molecules.

Using the present SANS data and density data taken from the literature, the Kirkwood-Buff integrals have been calculated using the formalism described in [5]. They are displayed in Figure 3. The rather high values of the solute-solute and water-water KBI gives quantitative characteristics for the preferential aggregation of the like species. The comparison of these KBIs with the earlier reported ones allows discriminating between the various datasets. It comes out that the presently obtained KBIs are in a fair agreement with those obtained from light scattering data: $G_{BE\text{-}BE} = 13000$ cm^3/mol at $t = 21^{\circ}$C and $X_{BE} = 0.05$ in the work of Kato [6]. But, our KBIs are in complete disagreement with two datasets obtained from vapor pressure measurements. In these latter studies the maximum values of the solute-solute KBIs are of about 500 cm^3/mol [3]. Such big discrepancies are not really surprising, knowing that the vapor pressure measurements and especially the data analysis for mixtures with strong deviations from ideality often suffer from large errors which are not easy to estimate.

These preliminary results of the present study indicate that aqueous solutions of rather large species can be correctly described by thermodynamic as well as scattering methods. Further, the experimental Kirkwood-Buff integrals for binary mixtures obtained from thermodynamic data only (i.e. using vapor pressure measurements), should be handled with certain caution, and should be checked by comparing them to results of scattering methods, wherever possible.

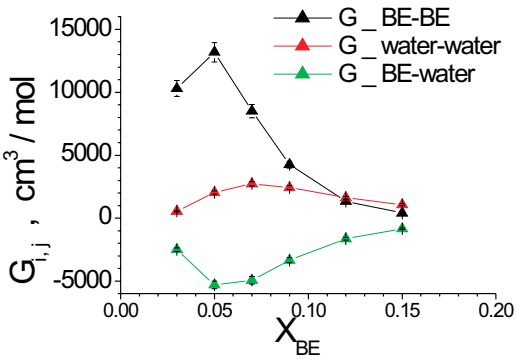

Fig.3. Kirkwood-Buff integrals in aqueous 2-butoxyethanol solutions at $t = 25^{\circ}$C.

References:

[1] E. Matteoli , L. Lepori: *J. Chem. Phys.* 80 (1984) 2856.
[2] I. Shulgin, E. Ruckenstein: *J. Phys. Chem. B* 103 (1999) 2496.
[3] Y. Marcus: *Monatsch. für Chemie* 132 (2001) 1387.
[4] G. D'Arrigo, J. Teixeira, R. Giordano, F. Mallamace: *J. Chem.. Phys.* 95 (1991) 2732.
[5] L. Almásy, G. Jancsó, L. Cser: *Appl. Phys.* A 74 (2002) S52.
[6] T. Kato: *J. Phys. Chem.* 88 (1984) 1248.

SANS Studies of Critical Phenomena in Ternary Mixtures

L.A.Bulavin, V.P.Kopylchuk, A.A.Khokhryakov (Kyiv Taras Shevchenko National University, Ukraine)
L.Almásy (KFKI Research Institute for Solid State Physics and Optics, Budapest, Hungary)
M.V.Avdeev (Frank Laboratory of Neutron Physics, JINR, Dubna, Russia)
V.M.Garamus (GKSS Research Centre, Geesthacht, Germany)

Nonionic binary mixtures having closed-loop immiscibility region on the temperature-concentration phase diagram (see fig.1, fig.2) belong to the universality class described by the 3D Ising model. Such system 3-methylpyridine/heavy water mixture with small addition of electrolyte is studied in our investigations by means of small-angle neutron scattering.

The first attempt to describe critical phenomena in mixtures was the Landau-Ginzburg theory - so called mean-field behavior model. This model is acceptable only for ionic solutions where long-range Coulomb forces are acting. In nonionic solutions the moving forces of the phase transformation at the lower critical temperature are short-range interactions described by 3D Ising

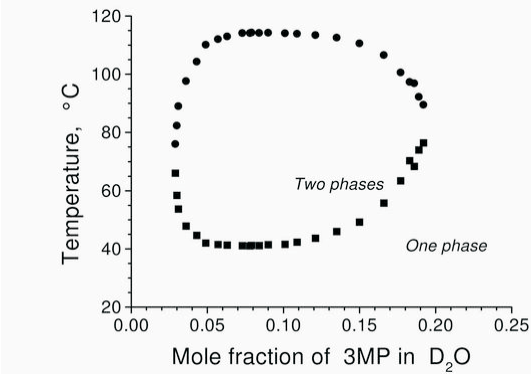

Fig.1. Closed-loop phase diagram of 3-methylpyridine/ heavy water mixture.

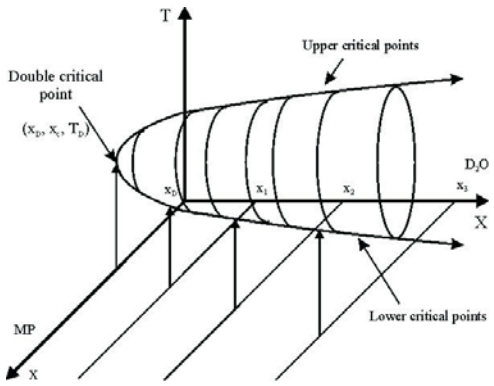

Fig.2. (T,X,x) surface of liquid-liquid immiscibility for [MP+HW+W] at constant pressure. The two-phase region disappeares at the double critical point (DCP: X_D, x_c,T_D).

model. Addition of a third component to the binary mixture causes changes of the critical parameters of the system: shift of the critical temperature, shift of the critical concentration, and deviation of the critical exponents. Thus for binary nonionic mixture with a small ionic additive the Ising-like behavior is not obvious [1]. The aim of our investigations was to detect possible deviations of critical exponents' values to the values within mean-field model.

Measurements of critical exponents in liquid mixtures by means of small-angle neutron scattering have long tradition [1,2]. The general form of the scattering intensity is given in the Ornstein-Zernike theory by the following formula:

$$I(q) = \frac{A\beta_T}{1 + (q\xi)^2} \qquad (1)$$

where q os the momentum transfer, A is a constant which does not depend on temperature, $\beta_T = \beta_{T,0} t^{-\gamma}$ is the osmotic compressibility $\xi = \xi_0 t^{-\nu}$ is the correlation length, and ξ_0 is the critical amplitude of the correlation length. Γ and ν are critical exponents, the theoretical values of which are respectively 1.24 and 0.63 in the 3D Ising model, and 1.0 and 0.5 in the mean-field approximation. The reduced temperature $t=(T_C-T)/T_C$ is used to characterize the distance from the critical point. Using Eq. (1) the temperature and external field dependence of the compressibility and the correlation length can be well followed by SANS.

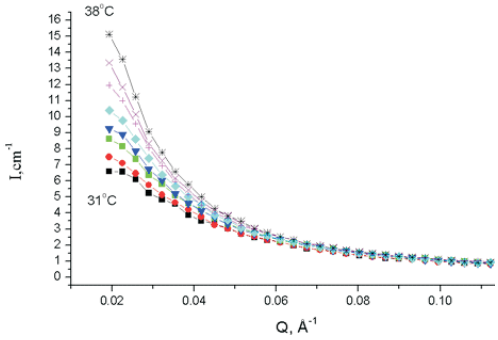

Fig.3. SANS spectra of binary mixtures 3MP - heavy water of critical composition.

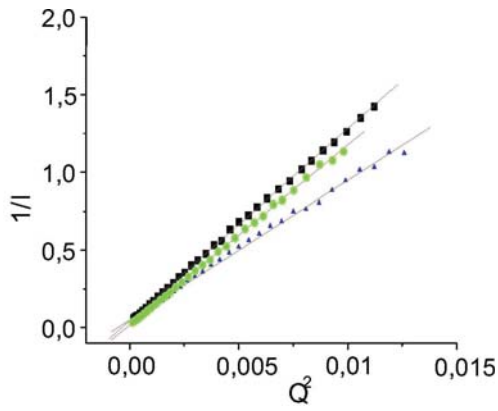

Fig.4. The shift of SANS curves due to the addition of electrolyte at the same reduced temperature.

We have performed SANS measurements on the system 3-methylpyridine - heavy water at critical composition (8.4 mol% of 3MP), and also on ternary systems 3MP-D_2O-salt, adding small amounts of NaCl and KCl. In general adding a third component to a binary mixture may change the critical concentration but we assume that this shift is small enough due to the small amount of added salt. The SANS measurements were performed on two different instruments: on the time-of-flight spectrometer YuMO in JINR, Dubna, and on the conventional SANS diffractometer Yellow Submarine in the KFKI, Budapest.

While approaching the critical temperature from below the scattering intensity increased due to the enhanced composition fluctuations (Fig.3). Contrary to our expectations, the scattering intensity was higher for higher salt concentrations at the same reduced temperature (Fig.4).

The scattering spectra were analyzed using the standard procedure of determination of the correlation lengths and osmotic compressibilities in the Ornstein-Zernike approximation (Eq. 1). From $\xi(t)$ and $\beta_T(t)$ their power-law dependence on the reduced temperature was determined. This analysis shows that in the ternary systems the critical exponents of the correlation length and the compressibility are higher than the corresponding quantities in the binary mixture (see the table). Instead of expected shifting down towards values characteristic for the mean-field behavior, the obtained critical exponents showed a negligible increase. Taking into account the experimental uncertainties we can state that the quasi-binary mixture preserves the Ising-like behavior and definitely does not show crossover to mean-field behavior.

The full article is presented in the ref. [3].

Table

Solution	ν	γ	R_{c0}, Å
3-MP+D_2O	0.60	1.20	2.3
3-MP+D_2O+KCl (0.08 % mas..)	0.68	1.30	2.9
3-MP+D_2O+KCl (0.3 % mas..)	0.76	1.38	4.2
3-MP+D_2O+NaCl (0.01 % mas..)	0.64	1.24	2.5
3-MP+D_2O+NaCl (0.4 % mas..)	0.72	1.32	3.8

References:

1. T. Narayanan, A. Kumar, Phys. Rep. 249 (1994) 135.
2. R. Schneider, L. Belkoura, J. Schelten, D. Woermann and B. Chu, Phys. Rev. B., 22, (1980) 5507
3. L.A.Bulavin, V.P.Kopylchuk, V.M.Garamus, M.V.Avdeev, L.Almasy, A.A.Hohryakov, Appl. Phys. A. 74 [Suppl.], (2002), 546-548

Mössbauer Study of Fe Thin Layers Irradiated with Kr Ions

S. Stichleutner, E. Kuzmann, K. Havancsák (Eötvös University, Budapest, Hungary)

The amorphization of crystalline materials due to heavy ion irradiation is a well known phenomenon. Metallic glasses can be usually prepared by the rapid quenching method. Metallic iron cannot be obtained in amorphous state using this conventional method of amorphization. However, amorphous iron was observed in sonochemically prepared materials as well as in swift heavy ion irradiated evaporated Fe multilayers.

The aim of the present work was to investigate the effect of the swift heavy ion irradiation on electrochemically deposited thin iron layers. The ultimate goal was to see whether electrochemically prepared crystalline Fe can be transformed into amorphous state by swift heavy ion irradiation. For this reason we have applied ^{57}Fe conversion electron Mössbauer spectroscopy.

The Fe electrodeposits were prepared in a continuous flow plating system. The composition of the electrolyte was 0.2 M $FeSO_4$, 120 g/l Na-gluc and 0.1 g/l Peptone. The deposition was performed on Cu substrate at pH=7.0, at 2 A·dm^2 and at 60 °C for 20 min.

The irradiation of samples was carried out with 246 MeV energy $^{86}Kr^{8+}$ ions at room temperature, at a current density of 0.5 мА·cm^{-2} and at a vacuum of about 10^{-5} Pa, with a dose of 10^{15} ion·cm^{-2} at the U-400 cyclotron of the Laboratory of Nuclear Reactions, JINR, Dubna, Russia.

The CEM spectra were recorded at room temperature by a conventional Mössbauer spectrometer (WISSEL) with a flowing gas (96% He, 4% CH_4) proportional counter and a ^{57}Co(Rh) source of 1.85 GBq activity. Isomer shifts are given relative to α-Fe. The evaluation of Mössbauer spectra was performed by least-square fitting of the lines using the MOSSWINN program.

Fig. 1 presents the ^{57}Fe Mössbauer spectra and the Mössbauer parameters of the electrodeposited Fe foils before and after the irradiation with 246 MeV energy $^{86}Kr^{8+}$ ions. The Mössbauer spectrum of the non-irradiated sample (Fig. 1a) was decomposed into a sextet (S1) and a doublet (D1). The sextet is the fingerprint of α-Fe. The doublet appears due to the oxidation of the surface, where the Mössbauer parameters are in the range characteristic of $Fe(OH)_3$ and FeOOH phases.

The ^{57}Fe Mössbauer spectrum of the sample irradiated with $^{86}Kr^{8+}$ ions with a fluence of 10^{15} ion·cm^{-2} (Fig. 1b) exhibit considerable changes compared to the non-irradiated one. The most striking change is the appearance of a new ferromagnetic component (sextet S2) with isomer shift around

0.14 mm·s^{-1} and effective magnetic induction around 26 T. This magnetically split pattern with six broad lines is considered as a superposition of a number of subspectra belonging to iron atoms being in slightly different microenvironments. In general, sextet S2 is typical for ferromagnetic materials being in amorphous state. The Mössbauer parameters of sextet S2 are similar to those found earlier for amorphous iron in samples prepared sonochemically from $Fe(CO)_5$ and by vacuum deposition of 70 nm thick films of iron onto Si wafers with subsequent heavy ion irradiation.

There are two main mechanisms of irradiation induced amorphization of crystalline solids: (1) continuous accumulation of defects which destabilize the crystal structure at some critical level, and (2) rapid quenching of irradiation induced liquid thermal spike regions. We assume that in our case the thermal spike, i.e. the electronic excitation mechanism is the dominant one. This is supported by results of the calculations made using the SRIM 2003 code, which show that the electronic stopping power is much higher than the nuclear stopping power in Fe irradiated with 246 MeV energy $^{86}Kr^{8+}$ ions. Further investigations to elucidate the effect of the irradiation conditions (fluence, energy and kind of ions) on the formation of amorphous Fe are in progress.

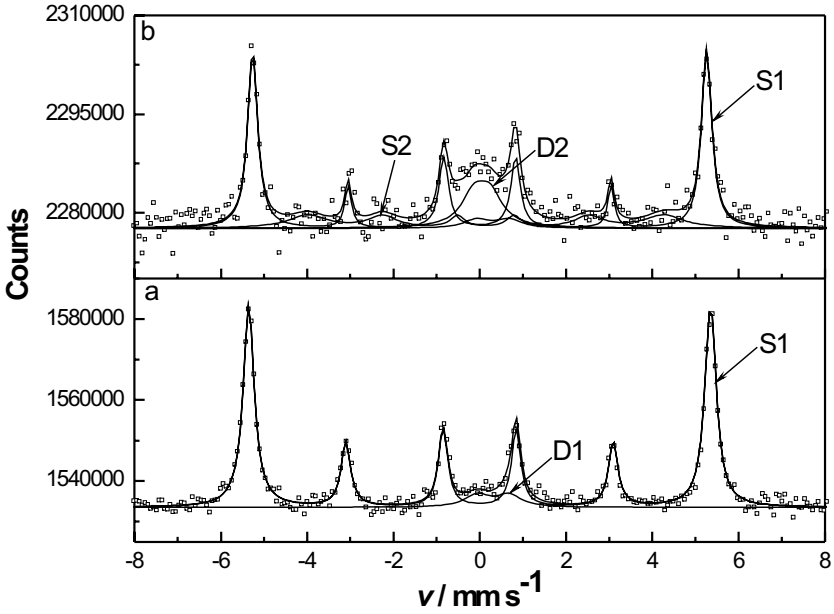

Fig.1. ^{57}Fe Mössbauer spectra of the electrodeposited Fe foils before (a) and after (b) the irradiation with 246 MeV energy $^{86}Kr^{8+}$ ions.

References:

1. E. Kuzmann, M. El-Sharif, C. U. Chisholm, G. Principi, C. Tosello, K. Havancsák, A. Vértes, K. Nomura, V. K. Garg, L. Takács, in Mössbauer Spectroscopy in Materials Science, edited by M. Miglierini and D. Petridis, Kluwer Academic Publishers, New York, 1999.
2. A. Perin, R. Gupta, G. Principi, C. Tosello, L. M. Gratton, E. Kuzmann, Z. Klencsár, Surf.Coat.Tech. 103-104 (1998) 93.
3. E. Kuzmann, G. Principi, C. Tosello, K. Havancsák, S. Stichleutner, I. Gerõcs, Z. Homonnay, A. Vértes, Nucl. Instr. and Meth. B 183 (2001) 425.
4. E. Kuzmann, M. El-Sharif, C. U. Chisholm, G. Principi, C. Tosello, A. Gupta, K. Havancsák, L. Takács, A. Vértes, Hyp. Int. 139-140 (2002) 193.
5. E. Kuzmann, K. Havancsák, C. Tosello, G. Principi, Gy. Dóra, Cs. Daróczi, A. Vértes, Radiat. Eff. Def. Solids 147 (1999) 255.
6. E. Kuzmann, S. Stichleutner, M. El-Sharif, C. U. Chisholm, L. Sziráki, Z. Homonnay, A. Vértes, Hyp. Int. 141-142 (2002) 425.
7. Klencsár, E. Kuzmann, A. Vértes, J. Radional. Nucl. Chem., 210 (1996) 105.
8. E. Kuzmann, S. Nagy, A. Vértes, Pure Appl. Chem. 75 (2003) 801.
9. E. Kuzmann, S. Stichleutner, M. El-Sharif, C. U. Chisholm, G. Principi, C. Tosello, K. Havancsák, I. Gerõcs, A. Vértes, Hyp. Int. C, 5 (2002) 591.

Surface Effects of Dense Ionization in Al_2O_3 and MgO

K.Havancsák (Eötvös University, Budapest, Hungary)
V.A.Skuratov (Flerov Laboratory of Nuclear Reactions, JINR, Dubna, Russia)
S.J. Zinkle (ORNL, Oak Ridge, USA)
A.E.Efimov (NT-MDT Co., Zelenograd, Moscow, Russia)

Surface topography changes in monocrystalline Al_2O_3 and MgO, induced by individual (0.5-3.4) MeV/amu Kr and Bi ions, has been studied as a function of ion energy, fluence, irradiation temperature and angle of ion incidence using atomic force microscopy (AFM) [1,2].

Microstructural and surface effects of dense ionization in radiation-resistant ceramics and oxide crystals are of considerable practical value. To date, only a few data concerning the microstructural response of nonfertile ceramics to ion irradiation of fission energy are available. An external bombardment with energetic ions offers a unique opportunity to simulate fission fragment-induced damages.

It was found that starting from a certain threshold ionizing energy loss value, the surface topography modification in Al_2O_3 and MgO targets consists of nanoscale conical-shaped hillocks associated with single ion impact [Fig. 1]. Fig. 2 shows mean hillock height as a function of incident electronic stopping power for sapphire and magnesium oxide crystals deduced from AFM images. A notable feature in the data presented is that, although hillocks are detected on MgO at lower energy deposition, their heights are considerably less than those found on Al_2O_3. The hillock height on sapphire

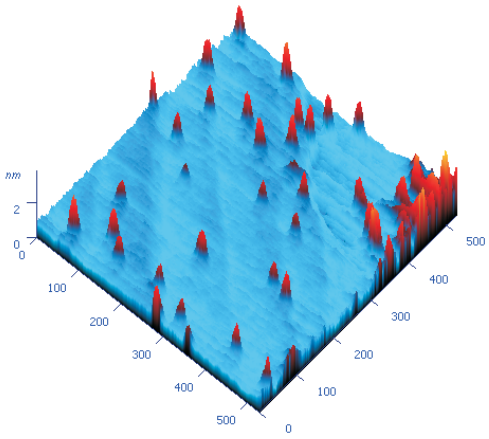

Fig.1. 3D AFM image of sapphire irradiated with Bi at 710 MeV. Ion fluence $2x10^{10}$ Bi/cm^2. Each ion hit induces one hillock.

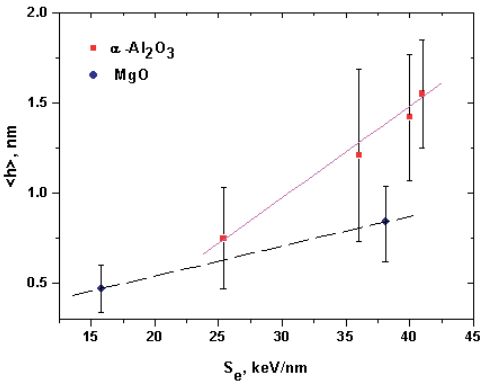

Fig.2. Variation of the mean hillock height on A_2O_3 and MgO with the energy deposition.

surface depends linearly on the incident electron stopping power and increases by two times on average when hillocks start to overlap.

Noticeable changes in defect shape are registered only under strong deviation from normal beam incidence (more than 60 degrees) and no specific features (radial coherent mass transport outwards from the track core) typical for shockwave-like mechanism were observed. In comparison to normal incidence the hillock shape became elongated to the ion entry direction, so its baseline profile changes roughly from the circle to ellipsoid, as can be seen from figure 3, where corresponding AFM phase images are given. Statistical analysis provides the ratio of mean baseline length to mean width as 1.6 to 1.

To check, if the hillock formation depended on macroscopic thermodynamic parameters, the irradiation effects at 80K and 300K were compared, taking into account that

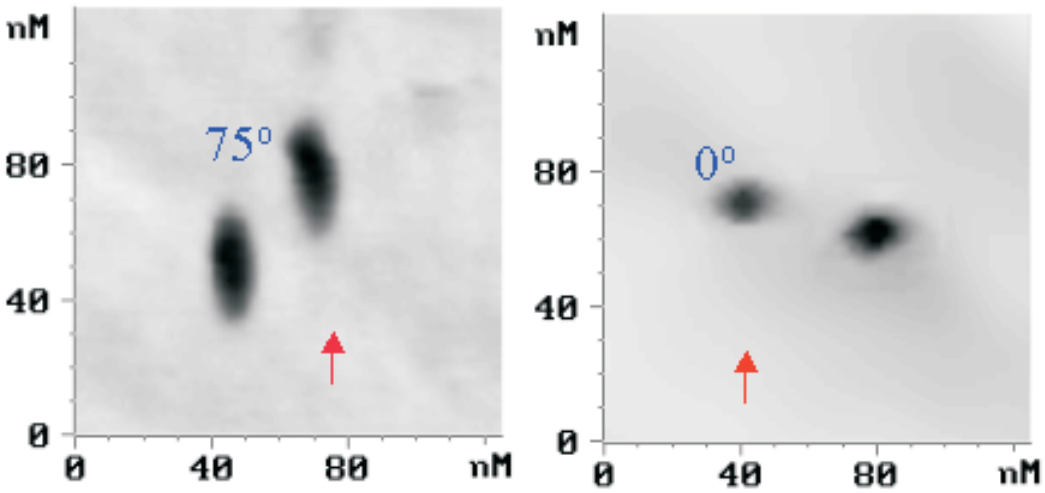

Fig.3. AFM phase images of A_2O_3 surfaces irradiated with 710 MeV Bi ions at 75° (a) and 0° (b) with respect to the surface normal. The arrows show ion beam direction.

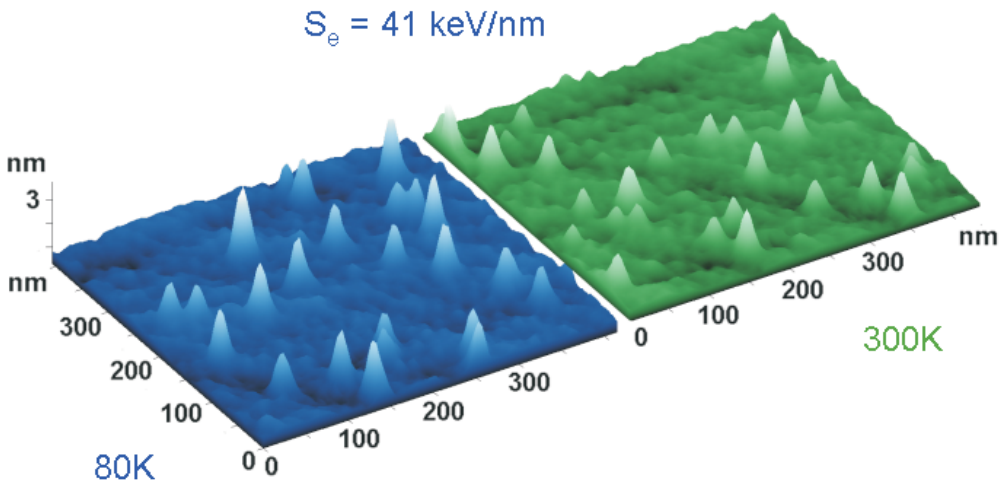

Fig.4. 3D AFM images of of A_2O_3 surfaces irradiated at 80 and 300K.

thermal conductivity of sapphire in this range varies from 1100 to 30-40 W/mK. The hillocks registered at both temperatures have the same geometry except for mean height, which is bigger at 80K, although this increase was very close to the experimental error in the measurements [Fig. 4].

To verify whether or not the ion track region in the material bulk was amorphous, high-resolution lattice imaging of sapphire specimen irradiated with 710 MeV Bi ions to a fluence of $7x10^{12} cm^2$ (plan view) was made. The microstructure of this target is given in figure 5. Electron diffraction and high-resolution TEM studies detected no evidence for an amorphous core of the ion track in Al_2O_5 irradiated at the mentioned energy, corresponding to electronic stopping power of 41 keV/nm. The micro-diffraction pattern in the ion track region was similar to the bulk diffraction pattern, although contrast associated with ion tracks was visible at medium magnification. Therefore, the hillock structures in sapphire are formed at electronic stopping powers less than required for amorphous latent track production in this material. Analysis of defect geometry versus ion incident angles showed that shockwave-like mechanism should be ruled out of consideration. As a possible reason, the Coulomb explosion is proposed as being responsible for the hillock formation.

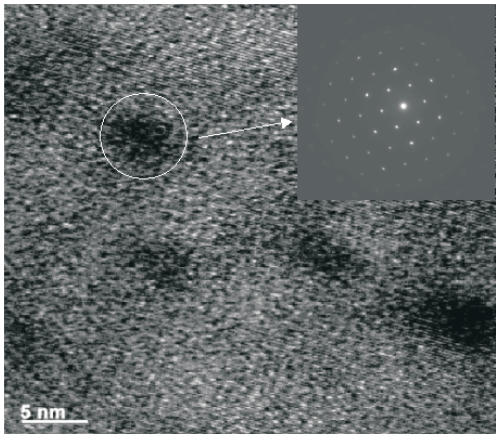

Fig.5. High-resolution lattice image of -A_2O_3 irradiated with 710 MeV Bi ions a fluence of 710^{12} cm^{-2} at room temperature (plan-view specimen). The average TEM track diameter is ~3 to 4 nm.

References:

1. V. A. Skuratov, S .J. Zinkle, A. E. Efimov, K. Havancsák. Nucl. Instr. Meth., B 203 (2003) 136
2. V. A. Skuratov, S .J. Zinkle, A. E. Efimov, K. Havancsák. Proceedings of the XIIIth International Conference on Surface Modification of Materials by Ion Beams, San Antonio, TX, September 21 - 26, 2003, to be published in Surface and Coating Technology.

Positron Lifetime and Doppler Broadening Study of Defects Created by Swift Ion Irradiation in Sapphire

L. Liszkay (Institut für Nukleare Festkörperphysik, Universität der Bundeswehr München, Germany)
L. Liszkay, Zs. Kajcsos (KFKI Research Institute for Particle and Nuclear Physics, Budapest, Hungary)
P. M. Gordo, A. de Lima (ICEMS, University Coimbra, Portugal)
K. Havancsák (Eötvös University, Budapest, Hungary)
V. A. Skuratov (Flerov Laboratory of Nuclear Reactions, JINR, Dubna, Russia)

Swift ions create a defect profile penetrating deep into a solid compared to the sampling range of typical slow positron beams, which may consequently study a homogeneous zone of defected materials. To investigate the defect population created by energetic ions, we studied α-Al_2O_3 single crystals irradiated with swift Kr ions by using conventional and pulsed positron beams. Samples irradiated with krypton at 245 MeV energy in a wide fluence range show nearly saturated positron trapping above $5x10^{10}$ ions cm^{-2} fluence, indicating the creation of monovacancies in high concentration. At $1x10^{14}$ ions cm^{-2} irradiation a 500 ps long lifetime component appears, showing the creation of larger voids. This threshold corresponds well to the onset of the overlap of the damage zones after Bi ion irradiation along the ion trajectories observed with microscopic methods.

Alumina is a widely used material both as a ceramic and as sapphire single crystal substrate for various thin layers. A better knowledge of lattice defects created by ion implantation or irradiation is important from a technological point of view. Positron annihilation (PA) spectroscopy has been extensively used to study implantation-induced defects in semiconductors and other materials. As positrons are uniquely sensitive and selective probes of vacancies, vacancy complexes and voids, their use can yield complementary information to other defect spectroscopy methods.

Swift heavy ions generate defects that penetrates several tens of microns into the substrate. Slow positrons with the routinely used 20-30 keV maximal beam energy (1.2-2.3 μm mean implantation depth) sample a relatively homogeneous region, far from the projected range of the implanted ions, where overlapping cascades complicate the defect creation process. In addition to the elastic damage, depending on the material and on the impinging ion, the high electronic stopping power (17 keV/nm, compared to the approximately 23 eV/nm nuclear stopping power) may create additional displacement damage through inelastic processes in the vicinity of the ion tracks.

Sapphire specimens with the (0001) axis oriented normal to the surface were irradiated at room temperature with 245 MeV Kr ions at the U-400 FLNR JINR cyclotron in Dubna, Russia. The ion flux was at about $2x10^8$ $cm^{-2}s^{-1}$.

PA lifetime measurements were performed at the pulsed positron beam facility in Munich at 16 keV beam energy. The contribution from positrons

annihilating on the sample surface after diffusion was found to be negligible in all samples but the unimplanted reference. Up to $5x10^6$ counts were collected per spectrum with a time resolution of 250 ps. To determine the positron diffusion length and gain chemical information on the defects through the core annihilation parameter, Doppler broadening (DB) measurements as a function of the positron energy were performed in Coimbra.

Three typical lifetime spectra are displayed in Fig. 1. In the unimplanted substrate a small component with longer lifetime is visible besides the short-lived bulk component, due to positrons diffusing back to the sample surface. At $5x10^{10}$ ions cm^{-2} fluence a single component dominates the spectrum, with a longer lifetime than that in the unimplanted reference sample. At $1x10^{14}$ ions cm^{-2} fluence a new, longer component appears.

The lifetime for the unimplanted sample is 145 ps, in agreement with that for sapphire single crystals from conventional positron lifetime measurements. Upon irradiation with a fluence of only $5x10^{10}$ ions cm^{-2}, the mean lifetime increases to 181 ps and levels off at 186 ps up to 10^{15} ions cm^{-2}. A further increase to 212 ps appears at 10^{14} ions cm^{-2} fluence. The increase in the mean lifetime is the result of the appearance of a new, 500 ps long lifetime component with 5 % intensity.

The constancy of the lifetime in a broad 10^{11}-10^{15} ions cm^{-2} fluence range can only be explained by a nearly saturated trapping effect. The 186 ps defect lifetime, similar to that measured in neutron irradiated sapphire and the corresponding Doppler S parameter

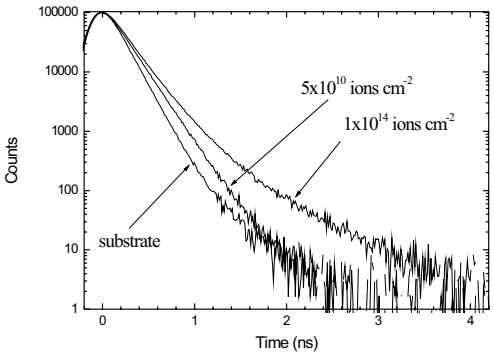

Fig.1. Positron lifetime spectra at 16 keV beam energy in the unimplanted substrate and at two different fluences.

which is 2.5 % higher than the bulk value can be attributed to a monovacancy, probably to a cation vacancy. The 500 ps lifetime (and the S/S_b=1.06 relative S parameter at 10^{14} ions cm^{-2} fluence) can only be explained by the creation of large vacancy clusters at high fluences.

The number of atomic displacements created can be estimated by using the TRIM code (Table 1), assuming a displacement energy of 51 and 31 eV per O and Al atoms, respectively. At $5x10^{10}$ ions cm^{-2} fluence approximately $3.5x10^{16}$ displacements cm^{-3} are created in the Al sublattice by the Kr ions in elastic processes. Due to recombination and possible local annealing the number of the remaining defects (C) must be in the low 10^{16} cm^{-3} range or even below that. Although the positron trapping coefficient is not known for monovacancies in sapphire, comparison with other materials implies that nearly saturated positron trapping would be unusual at the defect concentration shown above. Assuming τ_b=145 ps bulk lifetime, τ_d=186 ps defect lifetime, τ=180 ps mean lifetime and 10^{16} cm^{-3} vacancy concentration at $5x10^{10}$ ions cm^{-2} fluence, the μ trapping coefficient can be calculated as

$$\mu = \frac{1}{\tau_b C}\frac{\bar{\tau}-\tau_b}{\tau_d-\bar{\tau}} = 4\times10^{-6}\ \mathrm{cm^3 s^{-1}}.$$

Although we have hardly any data on the trapping coefficient of vacancies in oxides, this value appears to be very high compared to, e.g., to μ in semiconductors. The apparently unusually high value of the positron trapping coefficient implies that defects are created by inelastic processes as well. It was also found [1] that defects are created by collective electronic excitations during irradiation with swift ^{238}U ions. The threshold for defect creation through this inelastic process was estimated to be dE/dx=20 keV/nm. However, in the case of Kr irradiation, the electric stopping power is dE/dx= =17 keV/nm, i.e. our PA studies reveal significant defect creation by electronic excitation below the threshold given in Ref. 1.

The 500 ps component at 10^{14} ions cm^{-2} fluence indicates the emergence of a new defect, with a size of some ten atomic volumes, which may be created via the overlap of the ion tracks. As the mean distance between tracks is in the order of 3 nm and 1 nm at 10^{15} and 10^{14} ions cm^{-2}, respectively, we can estimate the effective track radius to be about 1 nm. This value is somewhat smaller than the 3 nm radius estimated on the basis of atomic force microscopy measurements. Another possible origin of the long-lived component can be the formation of grain boundaries or cracks due to thermoelastic stresses.

Positron annihilation measurements on swift heavy ion irradiated samples suggest the creation of considerable amount of vacancies by inelastic processes and the emergence of large voids at high irradiation fluences. However, since quantitative results on the positron trapping coefficient are not available for the present system, further studies are needed to quantify the defect creation process, just as well as for the unambiguous identification of the origin of the long lifetime component.

Table 1

Mean positron lifetime and number of displacements in the Al sublattice calculated by TRIM in sapphire after Kr irradiation at 245 MeV.

Fluence (ions cm^{-2})	Mean lifetime (ps)	Al displ. by TRIM (cm^{-3})
as received	145	0
$5x10^{10}$	180	$6x10^{16}$
10^{13}	186	$1.2x10^{19}$
10^{14}	212	$1.2x10^{20}$

References:

L.Liszkay, P.M.Gordo, K.Havancsák, V.A.Skuratov, A.deLima, Zs.Kajcsos, Materials Science Forum 445-446 (2004) 138

V. A. Skuratov, S. J. Zinkle, A. E. Efimov, K. Havancsak, Nucl. Instr. and Methods in Physics Research B 203 (2003) 136.

V. A. Skuratov, A. E. Efimov, D. L. Zagorskii, Physics of the solid state 44 (2002) 165.

Search for Long-lived States in Antiprotonic Lithium

J. Révai (KFKI Research Institute for Particle and Nuclear Physics, Budapest, Hungary)
V. B. Belyaev (Bogoliubov Laboratory of Theoretical Physics, JINR, Dubna, Russia)

The spectrum of the $(Li^{3+} + \bar{p} + 2e)$ four-body system was calculated in an adiabatic approach. The two-electron energies were approximated by a sum of two single-electron effective charge two-center energies as suggested in a recent work of Briggs & al. While the structure of the spectrum does not exclude the existence of long-lived states, their experimental observability is still to be clarified.

References:

PR **A 67**, *032507 (2003)*

Primary Population of Antiprotonic Helium States

J.Révai (KFKI Research Institute for Particle and Nuclear Physics, Budapest, Hungary)
N.V.Shevchenko (Bogoliubov Laboratory of Theoretical Physics, JINR, Dubna, Russia)

The question of initial distribution of antiprotonic helium atoms over the different final states (J, υ) in the capture reaction

$$\bar{p}+{}^4He \rightarrow ({}^4He^+\bar{p})_{J\upsilon}+e \qquad (1)$$

is one of the unsettled ones in the result-rich field of the study of metastable states of antiprotonic helium. While the existing approaches are based on a classical or semiclassical Monte-Carlo type treatment, we performed a full quantum mechanical calculation of the above process.

Full is meant in the sense that all degrees of freedom were taken explicitly into account, both initial and final configurations were true 4-body states. Of course, the full 4-body dynamics of this reaction is accounted for only in an approximate way. The partial cross sections can be written as

$$\sigma_{J\upsilon} = (2\pi)^4 \frac{K_f}{K_i} \mu_i \mu_f \int d\Omega_{\mathbf{K}_f} \left| \left\langle \Phi^f_{J\upsilon,\mathbf{K}_f} \right| V_f \left| \Psi^i_{He,\mathbf{K}_i} \right\rangle \right|^2,$$

where $\Psi^i_{He,\mathbf{K}_i}$ is exact 4-body scattering wave function corresponding to the initial (asymptotic) state

$$\Phi^i_{He,\mathbf{K}_i}(\mathbf{r}_1,\mathbf{r}_2,\mathbf{R}) = \Phi_{He}(\mathbf{r}_1,\mathbf{r}_2)\frac{1}{(2\pi)^{3/2}} e^{i\mathbf{K}_i\mathbf{R}}, \qquad (2)$$

while the final state $\Phi^f_{J\upsilon,\mathbf{K}_f}$, is taken in the form

$$\Phi^f_{J\upsilon,\mathbf{K}_f}(\boldsymbol{\rho}_1,\boldsymbol{\rho}_2,\mathbf{R}) = \Phi_{J\upsilon}(\boldsymbol{\rho}_1,\mathbf{R})\frac{1}{(2\pi)^{3/2}} e^{i\mathbf{K}_f\boldsymbol{\rho}_2} \qquad (3)$$

Here $\mathbf{r}_i$, are the vectors pointing from helium to the i-th electron, $\mathbf{R}$ is the vector between He and $\bar{p}$ and ρ_i are the Jacobian vectors connecting the electrons with the center of mass of the $He-\bar{p}$ system, $\Phi_{He}(\mathbf{r}_1, \mathbf{r}_2)$ is the He ground state wave function, while for the antiprotonic helium wave function $\Phi_{J\upsilon}(\rho_1, \mathbf{R})$ the Born-Oppenheimer form, which correctly reflects the main features of the final state, was used. The transition potential V_f is obviously the interaction missing from the final state.

For the Ψ^i we used two approximations: the plane wave Born approximation, when it was replaced by its asymptotic state (2) and an adiabatic Born-Oppenheimer type one:

$$\Psi^i_{He,\mathbf{K}_i} \approx \Phi_{He}(\mathbf{r}_1,\mathbf{r}_2;R)\chi^{(+)}_{\mathbf{K}_i}(\mathbf{R}), \qquad (4)$$

where $\Phi_{He}(\mathbf{r}_1, \mathbf{r}_2; R)$ is He wave function distorted by the antiproton at the distance R from it and $\chi^{(+)}_{\mathbf{K}_i}(\mathbf{R})$ is the scattering function of the antiproton in BO potential of the He atom.

The first part of the calculation is finished, while the second is in progress.

References:

Submitted to the XIX Few-Body Conference, Groningen, 23-23 August 2004 and to be published

Towards Thermodynamical Consistency of Quasiparticle Picture

T.S.Biro (KFKI Research Institute for Particle and Nuclear Physics, Budapest, Hungary)
A.A.Shanenko, V.D.Toneev (Bogoliubov Laboratory of Theoretical Physics, JINR, Dubna, Russia)

With the advent of RHIC and LHC, there is a growing need for a deeper understanding of various properties of the QCD matter at high temperature and finite density. At the moment, we are still far from a satisfactory level in this respect, even for equilibrium properties of quark-gluon plasma. Therefore, various phenomenological, QCD-motivated models are called up for describing the thermodynamics of highly excited nuclear matter and its equation of state.

By now, there is a number of simplified models for describing static hadron properties as well as a highly excited, deconfined state of quark matter, the quark-gluon plasma. A common feature of these models is that they all are based on a quasiparticle picture, considering isolated particle-like degrees of freedom and assuming that these quasiparticles are moving in a background mean field.

The present paper [1] concerns the quasiparticle description of the QCD thermodynamics with the particular emphasis on the mean-field treatment of in-medium strings.

We start with the general quasiparticle Hamiltonian

$$\hat{H} = \sum_i \sum_{\mathbf{k}} \varepsilon_{ki}(T,N) a^+_{\mathbf{k}i} a_{\mathbf{k}i} + V\Phi(T,n)\,. \qquad (1)$$

Here, $a^+_{\mathbf{k}i}$ and $a_{\mathbf{k}i}$ are the usual creation and annihilation operators for quasiparticles of the i-th sort with momentum $\mathbf{k}$. The background field $V\Phi(T, n)$ is nothing else but the energy of the quasiparticle vacuum. Generally speaking, it differs from the vacuum of primordial particles, which leads to the c-number term $V\Phi(T, n)$ appearing in Eq. (1).

Using temperature T and particle number densities $n_i = N_i/V$ as basic descriptive variables, the thermodynamical behavior and the appropriate equation of state can be derived from the corresponding thermodynamical potential, the free energy $F(V, N, T)$:

$$F \equiv Vf = T\sum_i \xi_i d_i \int \frac{d^3k}{(2\pi)^3} \ln\left(1 - \xi_i e^{-(\varepsilon_{ki}-\mu_i)/T}\right) + V\sum_i \mu_i n_i + V\Phi. \qquad (2)$$

Here $\xi_i = \pm 1$ is determined by the quasiparticle statistics, μ_i stands for the chemical potential of the quasiparticles of the i-th sort. To calculate the partition function in this case, the quasiparticle Hamiltonian (1) should be modified to

$$\hat{H}' = \hat{H} - \sum_i \mu_i \hat{N}_i\,, \qquad (3)$$

where is defined by Eq. (1).

If all the quantities of interest can be calculated only through the derivatives of this thermodynamical potential, one is prevented from encountering thermodynamical inconsistency. Problems arise, however, when calculation can proceed from a more fundamental level, some quasiparticle Hamiltonian to be dependent on temperature T and/or density n. As found in our paper [1], in the last case the following thermodynamical consistency requirements should be satisfied

$$\frac{\partial\Phi}{\partial T}+\sum_j d_j\int\frac{d^3k}{(2\pi)^3}\frac{\partial\varepsilon_{kj}}{\partial T}v_{kj}=0, \qquad (4)$$

$$\frac{\partial\Phi}{\partial T}+\sum_j d_j\int\frac{d^3k}{(2\pi)^3}\frac{\partial\varepsilon_{kj}}{\partial T}v_{kj}=0. \qquad (5)$$

Conditions of thermodynamical consistency (4) and (5) directly address to quasiparticle dispersion relation $\varepsilon_{kj}=\varepsilon_{kj}(T,n)$ and result in certain physical restrictions to the mean-field potential depending on the structure of quasiparticle spectra without coming into any detail of interaction between constituents. A few particular cases used in phenomenological treatments of equation of state were considered:

- A quasiparticle of the i-th sort moving in medium-dependent mean-field potential $U_i(T,n)$
$$\varepsilon_{ki}(T,n)=\omega_i(k)+U_i(T,n), \qquad (6)$$
- Quasiparticle spectra with an effective quasiparticle mass $m_i\equiv m_i(T,n)$
$$\varepsilon_{ki}(T,n)=\sqrt{k^2+m_i^2(T,n)}, \qquad (7)$$
- The mean field in Eq. (6) is scaled with some coupling constant, $U_i=g_iU$,
- The effective quasiparticle mass in Eq. (7) is also scaled as $m_i=g_iM(T,n)$. In particular, $M(T,n)$ can be the constituent quark mass, whereas g_i is the number of quarks in the baryon cluster of the i-th sort (i.e., forming baryons, mesons, hybrids, glueballs *etc*).

In addition to general restrictions to the phenomenological Hamiltonian due to the thermodynamical consistency a particular case of the mean-field model of strong pair interaction mediated by strings stretched between color charges was considered. Such a system is with long-range interaction, and only in-medium screening renders the problem treatable. The developed technique allows one to construct a thermodynamical potential in a self-consistent way and shows the rationality of our treatment of in-medium strings. Results of our consideration of the in-medium strings are found to be in reasonable agreement with the lattice data on QCD thermodynamics.

References:

[1] T. S. Biro, A. A. Shanenko, and V. D, Toneev, Yad. Fiz. **66** (2003) pp.982-996; [nucl-th/0102027]

Quasiparticles and Thermodynamical Consistency

T.S.Biro (KFKI Research Institute for Particle and Nuclear Physics, Budapest, Hungary)
A.A.Shanenko, V.D.Toneev (Bogoliubov Laboratory of Theoretical Physics, JINR, Dubna, Russia)

It is well-known that the concept of quasiparticles, proposed by Landau [1] and developed by Bogoliubov [2], is one of the most powerful tools of the present many-body physics. Quasiparticles provide us with understanding of such important phenomena as the superfluidity and superconductivity. Investigations of the Bose and Fermi gases, of the quantum liquids and of the solid state involves quasiparticle aspects, as a rule. At last, the most interesting for the heavy-ion community, the deconfinement problem is unlikely to be understood while ignoring these aspects. The deconfinement problem now is even formulated in terms of quasiparticles. Approaching the confinement, the characteristic quasiparticles are bound clusters of quarks and gluons. On the other hand, at high temperatures and large chemical potentials, unbound but effective quarks and gluons as quasiparticles play the major role. The intermediate regime is also explored in terms of the quark and gluon quasiparticles (constituent quarks, massive gluons, hadron-like excitations surviving the QCD phase transition etc.). Thus, as a rule, quasiparticle models of deconfinement are of special interest.

A distinctive feature of quasiparticles is that they have medium-dependent properties, for instance, a medium-dependent mass. When a quasiparticle picture is exactly derived from first principles there is no worry with the medium-dependent properties. However, turning to the thermodynamics of strong interactions, we cannot derive the quasiparticle properties exactly from first principles. Here physicists are forced *to construct* a quasiparticle picture, based, more or less, on their intuition with some additional assumptions involved. These assumptions are not easily to be controlled and lead often to a loss of the thermodynamical consistency. To escape such a serious trouble, some special constraints called *the thermodynamical-consistency relations* should be applied. The absence of a general form of the relations is quite inconvenient, because everybody who tries to develop a quasiparticle approach should explore its thermodynamical correctness from the very beginning by himself, which requires essential experience in thermodynamics. This is why inconsistent models are still met in the literature. So, the main aim of this report [3] is to demonstrate that the thermodynamical-consistency relations can be obtained in a quite general form being elegant and physically sound.

Let us consider a system governed by a Hamiltonian $\hat{H}$ depending on a set of parameters $\xi = \{\xi_1, \xi_2, \ldots\}$. The basic thermodynamical variables are the

temperature T, the volume V and the chemical potential μ. According to the prescriptions of the statistical mechanics, the parameter ξ has to lead to a minimum of the thermodynamical potential in equilibrium at any given T, V and μ. For the Grand Canonical Ensemble the thermodynamical potential is given by the following well-known formula:

$$\Omega(\xi;T,V,\mu) = -T\ln \mathrm{Tr}\, e^{-\frac{\hat{H}(\xi)-\mu\hat{N}}{T}} = -T\ln\sum_i \left\langle \psi_i(\xi)\left| e^{-\frac{\hat{H}(\xi)-\mu\hat{N}}{T}} \right| \psi_i(\xi)\right\rangle, \quad (1)$$

Where $\psi(\xi)$ stands for the eigenstates of the operator $\hat{H}(\xi)-\mu\hat{N}$. It is important to stress that ξ influences the thermodynamical potential in two ways: directly trough the Hamiltonian, and trough the eigenstates, which depend on this parameter, too. The extremum condition for ξ yields

$$\left.\frac{\partial\Omega}{\partial\xi}\right|_{T,V,\mu=const} = 0. \quad (2)$$

To make the next step in our consideration, we have generalized [3] *the Hellmann-Feynman theorem* to the finite temperature case

$$\delta\Omega(\xi) = \left\langle \delta\hat{H}(\xi)\right\rangle. \quad (3)$$

Here $\delta\Omega$ and $\delta\hat{H}$ are the infinitesimal changes of Ω and $\hat{H}$ with respect to ξ at any fixed T, V and μ. And $\langle ... \rangle$ means the statistical averaging.

Now, taking Eq. (2) in conjunction with the generalization of the Hellmann-Feynman theorem (3), one can arrive at the important equation

$$\left\langle \frac{d\hat{H}}{d\xi}\right\rangle = 0 \quad (4)$$

It is much more convenient to rearrange Eq. (4) in the following manner. As it has been mentioned above, the Hamiltonian depends on the thermo-dynamical variables only through the parameter ξ. So, for any of them ($a = T, V, \mu$) one has

$$\left\langle \frac{\partial\hat{H}}{\partial a}\right\rangle = \left\langle \frac{d\hat{H}}{d\xi}\frac{\partial\xi}{\partial a}\right\rangle = \frac{\partial\xi}{\partial a}\left\langle \frac{d\hat{H}}{d\xi}\right\rangle = 0.$$

Thus, operating with the Grand Canonical Ensemble we arrive at

$$\left\langle \frac{\partial\hat{H}}{\partial T}\right\rangle = \left\langle \frac{\partial\hat{H}}{\partial V}\right\rangle = \left\langle \frac{\partial\hat{H}}{\partial\mu}\right\rangle = 0. \quad (5)$$

The same procedure can be realized in the Canonical Ensemble with the result

$$\left\langle \frac{\partial\hat{H}}{\partial T}\right\rangle = \left\langle \frac{\partial\hat{H}}{\partial V}\right\rangle = \left\langle \frac{\partial\hat{H}}{\partial N}\right\rangle = 0, \quad (6)$$

where N denotes the number of quasiparticles. Equations (5) and (6) are the most general representations of *the thermodynamical consistency relations*. For homogeneous systems the following variant of the consistency relations is convenient to be used:

$$\left\langle \frac{\partial\hat{H}}{\partial T}\right\rangle = \left\langle \frac{\partial\hat{H}}{\partial n}\right\rangle = 0 \quad (7)$$

with $n = N/V$. Thus, introducing a quasiparticle Hamiltonian depending on some thermodynamical quantities, one should be careful and fulfill the relations (7). Otherwise, one faces some fault with the thermodynamics.

Restrictions following from these relations are illustrated in [3] by simple physical examples.

References:

[1] L. D. Landau, J. Phys. (USSR) **5** (1941) 71.
[2] N. N. Bogoliubov, J. Phys. (USSR) **11** (1947) 23, reprinted in *The many-body problem,* edited by D. Pines (W.A. Benjamin, New York, 1961) p. 76.
[3] A. A. Shanenko, T. S. Biro, and V. D. Toneev, Heavy Ion Collisions **18** (2003) 91-100.